Master's Thesis

Investigating the Effect of Antenna Polarization on the Performance of CoMP Systems based on Synchronous Multi-link Measurements

Sakib Bin Redhwan
Ahmad Shekhan

Department of Electrical and Information Technology,
Faculty of Engineering, LTH, Lund University, 2016.

Investigating the Effect of Antenna Polarization on the Performance of CoMP Systems based on Synchronous Multi-link Measurements

Sakib Bin Redhwan
sakibsejan@gmail.com
Ahmad Shekhan
amad.shekhan@gmail.com

Department of Electrical and Information Technology
Lund University

Advisor: Dr. Ghassan Dahman

9th June 2016

Printed in Sweden
E-huset, Lund, 2016

Abstract

In this master thesis work, the effect of polarization, at the Base Station (BS) side, on the performance of multi-user Coordinated Multipoint (CoMP) systems is studied. This study was performed using synchronous multi-link measurements that took place at the campus of the faculty of Engineering, LTH, Lund University, Lund, Sweden, where two different BS setups were studied.

In the first setup, one BS provided with one antenna array consisting of four antenna elements, was used. The antenna aperture size was varied from 0.17 m to 24 m, where different antenna polarizations (single- and cross-polarized arrangements) were considered. In the second setup, we use two BSs located 60 m apart, each of which is provided with two co-located antenna elements spaced by half a wavelength. Two antenna polarizations at the BS are studied: single- and cross-polarized arrangements. In both setups, four virtual users, spaced 0.5 m apart with one cross-polarized antenna were considered.

For each setup, the user Multiple Input Multiple Output (MIMO) channels are used to evaluate the sum-rate capacity of the system, where the minimum mean square error (MMSE) beamforming at both the BS and the Mobile Station (MS) was used. Furthermore, in the second setup, the influence of user hand and torso into the MS antenna patterns and hence into the resulting performance was incorporated.

For the first setup, i.e., using one BS antenna with variable aperture, it was found that: 1) using cross-polarized antenna elements at the BS improves the sum-rate capacity by about 35% and 72% in Non Line of Sight (NLOS) and Line of Sight (LOS), respectively, if the aperture of the antenna array is small (less than 1 m). 2) Increasing the BS array aperture gives better sum-rate capacity to a certain point, then the improvement saturates. 3) If the BS array aperture is "large enough", then the performance improvement gained from using BS cross-polarized antennas is insignificant compared to using single-polarized ones. For the second setup, i.e., using two BSs each of which is provided with co-located antennas with half a wavelength inter-element spacing, it was found that: the cross-polarized antenna configuration improves the ergodic sum-rate capacity about 50% compared to the single polarization configuration. In addition, increasing the number of antenna (from 1 to 2) at the MS side yielded an improvement of 43% in sum-rate capacity.

Acknowledgement

First and foremost, praises and thanks to the Almighty creator, for His showers of blessings throughout our work to complete this thesis successfully.
We would like to show our sincere gratitude to our advisor Dr. Ghassan Dahman for his thorough help, guidance and insightful comments during the thesis project, which enabled us to finish our work. Sincere thanks to our examiner Dr. Fredrik Rusek for the feedback and suggestions on the report. Also, a special thanks to Prof. Fredrik Tufvesson for giving us the opportunity to work in this project. Our appreciation to Jose Flordelis for providing the Multi-link measurement data.
We are grateful to Dr. Fredrik Harrysson of Ericsson AB for providing the measurement data of the user antenna patterns and the phantom.
We would also like to thank our families for the unconditional love, endless support and encouragement at all times.
Sakib would like to especially thank his wife for her forbearance and endurance during the study period. He would also like to pay gratitude to Swedish Institute (SI) for providing scholarship to study in this master program.

Lund, June 2016
Sakib Bin Redhwan & Ahmad Shekhan

Contents

1 Introduction **1**
- 1.1 **Background** . . . 1
- 1.2 **Previous work** . . . 4
- 1.3 **Objectives** . . . 4
- 1.4 **Contributions** . . . 5
- 1.5 **Thesis structure** . . . 5

2 MIMO channel analysis **7**
- 2.1 **Derivation of MIMO channel matrix** . . . 8
- 2.2 **Estimation of the channel parameters using Space-Alternating Generalized Expectation-Maximization (SAGE)** . . . 8
- 2.3 **Channel metrics** . . . 10

3 Measurement description **13**
- 3.1 **Measurement setup** . . . 13
- 3.2 **Extracting MIMO user channels in setup I** . . . 17
- 3.3 **Extracting MIMO user channels in setup-IIA** . . . 20
- 3.4 **Extracting MIMO user channels in setup-IIB** . . . 22

4 MU-MIMO BC capacity **29**
- 4.1 **Signal model** . . . 29
- 4.2 **Capacity calculation** . . . 29
- 4.3 **Linear precoding techniques** . . . 30

5 Results and analysis **33**
- 5.1 **Setup-I: Single BS with variable aperture** . . . 33
- 5.2 **Setup-IIA: Two BSs with fixed aperture** . . . 38
- 5.3 **Setup-IIB: Two BSs with fixed aperture & user antenna pattern** . . . 41

6 Conclusion **49**

7 Future works **51**

Bibliography **53**

List of Figures

1.1 Uplink (MAC) and Downlink (BC) channels of MU-MIMO. 3

2.1 SAGE algorithm 9

3.1 Antennas at the receiver and at the BS. (a) receiver antenna: stacked uniform cylindrical array with 64 cross-polarized antenna elements arranged in four rings. (b) BS antennas: co-located arrangement used in setup-II with inter-patch spacing of $\lambda/2$ (back view). (c) BS antennas: mounted on a tripod to facilitate adjusting the inter-patch spacing for setup-I, the photo is with inter-patch spacing of 1 m (back view). 14

3.2 Aerial photo of the measurement area illustrating setup-I. BS antennas are indicated with the blue circles all placed at one BS. The receiver measurement routes are plotted in dashed blue lines: Route 1 is mainly LOS; Route 2 and Route 3 are mainly NLOS. 15

3.3 Aerial photo of the measurement area illustrating setup-II. BS-E and BS-S are indicated with the large green circles. Each BS is equipped with co-located antenna arranged as depicted in 3.1.b. The receiver measurement route is indicated by the small red circles. 16

3.4 Schematic diagram of BS (Setup-I) 17

3.5 Schematic diagram of BS elements Vertical polarization (V.Pol.) . . . 18

3.6 Schematic diagram of BS elements Horizontal Polarization (H.Pol.) . 18

3.7 Schematic diagram of BS elements Cross polarization-I (Co.Pol.I) . . 19

3.8 Schematic diagram of BS elements Cross polarization-II (Co.Pol.II) . . 19

3.9 Schematic diagram of Mobile station antennas 20

3.10 Schematic diagram of BS (for both Setup-IIA and SetupII-B) 20

3.11 Handset positions in hand (a) Position1, (b) Position 2, (c) Position 3. 1, 2, 3, 4 represents the element numbers (Talk mode) 22

3.12 Radiation pattern of antenna element 1 of position TM2 (vertical gain in Talk Mode) 23

3.13 Radiation pattern for all elements. (a) Element 1, TM1, (b) Element 2, TM1, (c) Element 1, TM2, (d) Element 2, TM2, (e) Element 1, TM3, (f) Element 2, TM3 24

3.14 Radiation pattern of antenna element 1 of position DM2 (vertical gain in Browse Mode) 25
3.15 Radiation pattern for all elements. (a) Element 1, DM1, (b) Element 2, DM1, (c) Element 1, DM2, (d) Element 2, DM2, (e) Element 1, DM3, (f) Element 2, DM3 26

5.1 Ergodic sum-rate capacities using MMSE beamformer for different BS antenna array aperture: a) Route 1, b) Route 2, c) Route 3, d) All Routes 34
5.2 Ergodic sum-rate capacities using ZF beamformer for different BS antenna array aperture: a) Route 1, b) Route 2, c) Route 3, d) All Routes 35
5.3 Ergodic sum-rate capacities using general coordinated beamforming for different BS array aperture: a) Route 1, b) Route 2, c) Route 3, d) All Routes 36
5.4 Condition number for different BS antenna array aperture: a) 0.17 m, b) 0.34 m, c) 1.5 m and d) 12 m 37
5.5 CDFs of sum-rate Capacity (MU-MISO) 39
5.6 CDF of sum-rate capacity (MU-MIMO) 40
5.7 Condition number (singular value spread) of the channels, (a) MU-MISO, (b) MU-MIMO 40
5.8 CDF of Channel Matrix Collinearity (Talk Mode) 42
5.9 CDF of Condition Number Ratio (Talk Mode) 42
5.10 CDF of sum-rate capacity (Talk Mode) 43
5.11 CDF of the condition numbers of the equivalent channels 44
5.12 CDF of Ratio of the Singular values (Talk Mode), (a) H.Pol. (b) V.Pol. (c) Co.Pol. configurations 44
5.13 CDF of Channel Matrix Collinearity (Browse mode) 45
5.14 CDF of Condition Number Ratio (Browse mode) 46
5.15 CDF of sum-rate capacity (Browse mode) 46
5.16 CDF of the condition numbers of the equivalent channels 47
5.17 CDF of Ratio of the Singular values(Browse Mode), (a) H.Pol. (b) V.Pol. (c) Co.Pol. configurations 47

List of Tables

4.1 Algorithm for general coordinated beamforming 32

5.1 Summary of antenna element polarization and array aperture effect on sum-rate capacity 38
5.2 Summary of antenna element polarization effect on sum-rate capacity for Setup-IIA 41
5.3 Summary of antenna element polarization effect on sum-rate capacity for Setup-IIB 48

List of Abbreviations

AOA	Angle of Arrival.
AOD	Angle of Departure.
BD	Block Diagonalization.
BS	Base Station.
CB	Coordinated Beamforming.
CDF	Cumulative Distribution Function.
CoMP	Coordinated Multipoint.
CS	Coordinated Scheduling.
CSI	Channel State Information.
CU	Central Unit.
DPC	Dirty Paper Coding.
ICI	Inter-Cell Interference.
JP	Joint Processing.
JT	Joint Transmission.
	.
LOS	Line of Sight.
MIMO	Multiple Input Multiple Output.
MIMO-BC	MIMO Broadcast Channel.
MIMO-MAC	MIMO Multiple Access Channel.
MISO	Multiple Input Single Output.
MMSE	Minimum Mean Square Error.
MPC	Multipath Components.
MRC	Maximum Ratio Combining.
MS	Mobile Station.
MU-MIMO	Multi-User MIMO.
NLOS	Non Line of Sight.

PIFA	Plannar Inverted F Antenna.
Rx	Receiver.
SAGE	Space-Alternating Generalized Expectation-Maximization.
SDMA	Space Division Multiple Access.
SINR	Signal to Interference to Noise Ratio.
SISO	Single Input Single Output.
SNR	Signal to Noise Ratio.
SU-MIMO	Single-User MIMO.
Tx	Transmitter.
TxUs	Transmit Units.
ZF	Zero Forcing.

Chapter 1

Introduction

1.1 Background

1.1.1 MIMO

Since the demands for higher capacity has almost fully exploited time and frequency domains, the spatial domain can be used to increase the capacity of wireless systems. It has been shown that MIMO system promises a considerable increase in capacity of cellular systems [1]. Having rich scatterer environment yields independent parallel channels between the transmitter and receiver resulting in linear increase of capacity. A straightforward way to ensure rich environment is to use spatially separated antennas at the BS and the MS. Although increasing the number of antennas increases capacity, this solution is not feasible at the MS due to limited size and cost. A remedy for this dilemma is to use cross-polarized antennas. Moreover, MIMO increases the reliability of the system through diversity gain. Sending the same information from multiple transmit antennas increase the chances that the information reaches the receiver. Some of the signals might undergo deep fades, while other signals experience less fading and thus reach the receiver with better signal quality and hence increase the reliability of the system. The conventional single-antenna technology might not be able to provide certain quality of service levels with reliable data rate. MIMO technology, where receivers are more complex, can mitigate fading by exploiting angular spread to distinguish Multipath Components (MPC) with different Angle of Arrival (AOA). Furthermore, MIMO technology can improve bit error performance, enhance data rate without increasing transmit power and increase Signal to Noise Ratio (SNR) [1] [2]. Using multiplexing technique to increase the data rate, the BS can transmit independent data from each antenna and these transmitted signals are combined over the propagation channel. The receiver equipped with multiple antennas and using interference cancellation techniques such as Zero Forcing (ZF) and Minimum Mean Square Error (MMSE) equalization, is able to separate the signals.

1.1.2 Single-User MIMO

Conventional MIMO systems supporting a single user are referred to as Single-User MIMO (SU-MIMO) or point-to-point MIMO, where a BS with multiple (M_T) transmit antennas communicates with a single MS with multiple (M_R) receive antennas. Time-frequency resources in SU-MIMO are dedicated to a single MS. The capacity for SU-MIMO channels is easier to derive [1] compared to that of Multi-User MIMO (MU-MIMO) especially when the channel is not known at the transmitter. SU-MIMO system has a defined link capacity whereas the capacity of MU-MIMO is characterized in terms of capacity region [1].

1.1.3 Multi-User MIMO

In cellular telephony, the scheme where the MIMO BS is serving many users simultaneously in the same frequency channel, is referred to as MU-MIMO. MU-MIMO implies frequency reuse within a cell (or sector) [1]. In MU-MIMO systems a BS with multiple (M) antennas communicates with K users with one or more antennas. Multiple connections on a single conventional channel are supported by MU-MIMO and different users are identified by spatial signatures. Furthermore, it mitigates the interference from adjacent cells, similar to Space Division Multiple Access (SDMA) technology [3]. SU-MIMO however, does not suffer from co-channel interference. Channel State Information (CSI) is needed for MU-MIMO to increase the system throughput. Since SU-MIMO has only one user and thus no co-channel interference, it performs better than MU-MIMO at low SNR. The forward link, where the BS transmits to the terminals, is called MIMO broadcast channel (MIMO-BC) and the reverse link, where the terminals transmit to the BS, is called MIMO multiple access channel (MIMO-MAC). MU-MIMO links are depicted in Figure 1.1

1.1.4 MU-MIMO vs SU-MIMO

In SU-MIMO, the BS communicates with a single user having one or more antennas, in contrast to MU-MIMO where the BS communicates with multiple users. MU-MIMO users communicate over the same time-frequency resource simultaneously which improves the system performance. SU-MIMO does not suffer from co-channel interference which is the case for MU-MIMO. Approaches such as beamforming could be used to mitigate the effect of interference. In downlink, MU-MIMO requires perfect CSI to achieve high throughput. In fact, the throughput of MU-MIMO and SU-MIMO systems depend on the SNR level. SU-MIMO performs better at low SNR whilst MU-MIMO provides better performance at high SNR level [3].

MU-MIMO has the following advantages over SU-MIMO [4]-[5]:
1) The BS can obtain spatial multiplexing gain irrespective of number of antennas at the user terminals, allowing to reduce cost in the latter.
2) Antenna correlation has smaller degrading effect on the performance of MU-MIMO since multiuser diversity is possible.

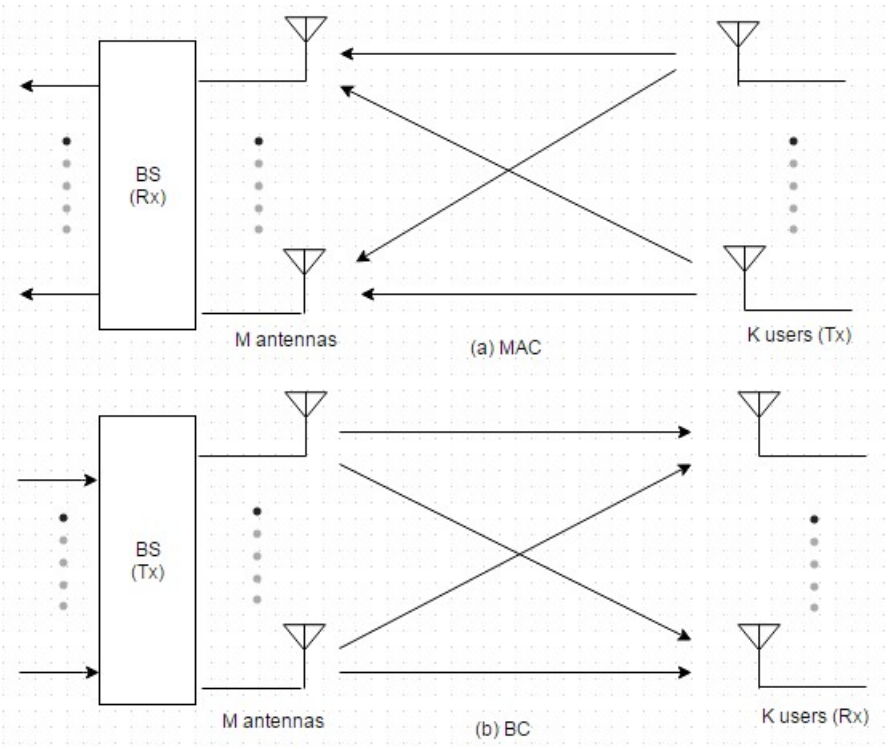

Figure 1.1: Uplink (MAC) and Downlink (BC) channels of MU-MIMO.

3) Since users are spatially separated, the correlation between antennas tend to be low.

1.1.5 Coordinated Multipoint (CoMP)

The increasing demand for higher data rates and better quality of service, given the scarce radio resources, forces wireless networks to advance in order to accommodate the requirements while improving spectral efficiency and coverage area. MIMO transmission can increase capacity linearly when independent parallel channels exist. Furthermore, it can greatly increase capacity when the signal-to-interference-plus-noise ratio (SINR) is high. However, this condition is not met at the cell edges [6]. MU-MIMO technology was developed to further improve the capacity and spectral efficiency of cellular networks [7] however, intercell-interference (ICI) limits this improvement and increasing the number of antennas might not improve the performance. Cell-edge users' signal quality can degrade dramatically due to ICI, since each BS transmits signal to the users within its cell coverage, limiting the capacity of the downlink channel in conventional cellular networks [8]. CoMP technique however mitigates or exploits the ICI since the BSs are connected via a high-speed backbone such that cooperation

and exchange of information is possible between BSs [8][9]. In CoMP, users are served by geographically separated BSs. Downlink CoMP is categorized into two schemes: Coordinated scheduling/beamforming (CS/CB) and Joint Transmission (JT). (CS/CB) cancels interference whereas (JT) scheme exploits interference. CoMP technology however comes at the cost of increased complexity and accurate channel information exchange [10][11]. CoMP is classified into: Inter-site CoMP and Intra-site CoMP. In Intra-site CoMP, the coordination is performed between sectors of the same BS. In Inter-site CoMP, which will be the focus of this work, the coordination is among geographically separated BSs. In (CS/CB), user data is available at and transmitted from only one BS, while user scheduling and beamforming decisions are made with coordination among BSs. In this scheme the coordinated BSs share only channel state information (CSI), thus it has lower feedback overhead compared with JT scheme. The BS creates beams such that it increases the signal strength toward the desired user as well as decreases interference toward the user in the adjacent cell. The user data, in JT scheme, is available at multiple BSs and is simultaneously transmitted to the user. JT scheme requires a large amount of signal overhead on the backhaul, since both data and CSI need to be shared between BSs and the central unit (CU) [9][10][11][12]. The BSs act like a distributed antenna system in JT scheme, where they form beams towards users in the coverage area. Using all BS antennas to create these beams, ICI is exploited and turned into desired signals.

1.2 Previous work

Capacity of CoMP has been studied in several papers. In [13], the authors showed that for coherent measurements, the average multi-user sum rate is increased by 37% and 91% for two and three users, respectively. For non-coherent measurements, [14] showed that the cell capacity with BS cooperation is approximately five times higher compared to that of the traditional frequency reuse scheme. [15] studied the effect of BS antenna element spacing on MU-MIMO separation, where it is also shown the improved capacity due to BS cooperation. In [16], the user impact on MIMO channel is studied and it is shown that the effect of the user causes an efficiency loss between 1.4-4.8 dB depending on user operation.

1.3 Objectives

The objective of this thesis work is to study the effect of antenna polarization on the performance of a CoMP system. During this work, the effect of BS antenna inter-element distance on sum-rate capacity is also studied. The performance is studied in terms of sum-rate capacity for non-ideal precoders. Furthermore, to study the impact of MS position on the MIMO channel, two different MS positions were evaluated, namely talk position and browse position.

1.4 Contributions

Through the sum-rate capacity calculation of MIMO-BC in this work, the effect of polarization and BS inter-element distance on the performance of the system has been studied. Also, this is the first work that we are aware of where the effect of antenna polarization on sum-rate capacity of CoMP system incorporating user influence is experimentally evaluated.

1.5 Thesis structure

The rest of the thesis is organized as follows. An introduction to MIMO channels and a few related channel metrics are introduced in Chapter 2. Chapter 3 describes the measurement setup and equipment description. Sum-rate capacity calculation of the MIMO-BC is described in Chapter 4. Results and analysis of the work are given in Chapter 5. Finally, conclusions drawn and future work are presented in Chapter 6 and Chapter 7, respectively.

Chapter 2

MIMO channel analysis

A system, where the transmitter and/or the receiver have an array of antenna, i.e. multiple closely-spaced antennas, is called multiple-antenna or MIMO system. The MIMO channel matrix with M_T transmit antennas and M_R receive antennas can be written as $\mathbf{H}$ and the input-output relationship modelled as:

$$\mathbf{Y} = \mathbf{H}\mathbf{x} + \mathbf{n}, \tag{2.1}$$

where $\mathbf{x}$ and $\mathbf{Y}$ are the transmitted and the received signals, respectively. $\mathbf{H}$ is the MIMO channel matrix and $\mathbf{n}$ is the white Gaussian noise. Details about this system model, i.e. the dimensions of $\mathbf{Y}$, $\mathbf{x}$ and $\mathbf{n}$ are described in Chapter 4.

In wireless networks, signals arrive at the receiver via different paths. The multipath signals have different time delays, angles of departure and arrival, as well as different attenuations. This property causes transmission channels to be complex. Let L be the number of multipath signals between the transmitter and the receiver, then the double-directional impulse response of the channel can be written as:

$$h(t, \tau, \mathbf{\Omega_t}, \mathbf{\Omega_r}) = \sum_{k=0}^{L-1} h_k(t, \tau, \mathbf{\Omega_t}, \mathbf{\Omega_r}). \tag{2.2}$$

In Equation (2.2), the notations are as follows,
t represents the time variable. At any given time t, the received power varies as a function of the delay τ. $\mathbf{\Omega_t}$ and $\mathbf{\Omega_r}$ represent angles of departure and arrival, respectively. Each signal leaves the transmitter and reaches the receiver in certain direction. This can be thought of as directional distribution of energy at both sides of the channel. $\mathbf{\Omega_t}$ and $\mathbf{\Omega_r}$ contain both azimuth and elevation angles, (θ_t, ϕ_t) and (θ_r, ϕ_r). The Angle of Departure (AOD) $\mathbf{\Omega_t}$ is uniquely determined by its spherical coordinates (i.e., the azimuth θ_t and elevation ϕ_t) on a sphere of unit radius according to the relationship:

$$\mathbf{\Omega_t} = [cos\theta_t sin\phi_t, sin\theta_t sin\phi_t, cos\phi_t]^T. \tag{2.3}$$

Here, $[.]^T$ represents matrix transpose. The AOA ($\mathbf{\Omega_r}$) is defined analogously.

Equation (2.2) assumes isotropic antennas at both transmitter and receiver sides. In other words, it does not depend on antenna pattern and system bandwidth. Taking antenna patterns into account and filtering over a certain bandwidth (B), Equation (2.2) can be re-written as:

$$h_{a,B}(t,\tau,\mathbf{\Omega_t},\mathbf{\Omega_r}) = f_r(\tau) * [g_r(\mathbf{\Omega_r})h(t,\tau,\mathbf{\Omega_t},\mathbf{\Omega_r})g_t(\mathbf{\Omega_t})] * f_t(\tau), \quad (2.4)$$

where $g_r(\mathbf{\Omega_r})$ and $g_t(\mathbf{\Omega_t})$ are the complex field-pattern of the receive and transmit antenna elements, respectively. $f_t(\tau)$ and $f_r(\tau)$ are the transmit and receive filters of the system, respectively.

In this chapter, a brief introduction of the structure of the channel matrix is described. Also, one of the many algorithms used to estimate the parameters of MPCs, namely the SAGE algorithm and few metrics for analyzing and understanding the channel is described as well.

2.1 Derivation of MIMO channel matrix

The MIMO channel matrix $\mathbf{H}$ of Equation (2.1) can be written as-

$$\mathbf{H} = \begin{bmatrix} h_{11} & h_{12} & \dots & h_{1,M_T} \\ h_{21} & h_{22} & \dots & h_{2,M_T} \\ \vdots & \vdots & \vdots & \vdots \\ h_{M_R,1} & h_{M_R,2} & \dots & h_{M_R,M_T} \end{bmatrix}$$

where $h_{n,m}$ denotes the channel between the n^{th} receive and m^{th} transmit antenna element and is a function of time and delay. Thus, the channel matrix can be written as [17]-

$$\mathbf{H}(t,\tau) = \begin{bmatrix} h_{11}(t,\tau) & h_{12}(t,\tau) & \dots & h_{1,M_T}(t,\tau) \\ h_{21}(t,\tau) & h_{22}(t,\tau) & \dots & h_{2,M_T}(t,\tau) \\ \vdots & \vdots & \vdots & \vdots \\ h_{M_R,1}(t,\tau) & h_{M_R,2}(t,\tau) & \dots & h_{M_R,M_T}(t,\tau) \end{bmatrix}, \quad (2.5)$$

where

$$h_{n,m}(t,\tau) \triangleq \iint h_{n,m}(t,\mathbf{P_t}^{(m)},\mathbf{P_r}^{(n)},\tau,\mathbf{\Omega_t},\mathbf{\Omega_r})d\mathbf{\Omega_t}d\mathbf{\Omega_r}, \quad (2.6)$$

and t, τ, $\mathbf{\Omega_t}$, $\mathbf{\Omega_r}$, $\mathbf{P_t}^{(\mathrm{m})}$, $\mathbf{P_r}^{(\mathrm{n})}$ are the time, delay, AOD, AOA, location of the m^{th} transmit antenna element and location of the n^{th} receive antenna element, respectively.

Equation (2.6) originated from the double directional channel model [17] and the inherent assumption is that the transmit and receive antennas are omnidirectional. The directivity of the antennas and the filtering effects of the system can be incorporated by using Equation (2.4).

2.2 Estimation of the channel parameters using SAGE

The parameters of the MPCs ($\boldsymbol{\tau}$, $\mathbf{\Omega_t}$, $\mathbf{\Omega_r}$, $\boldsymbol{\alpha}$, $\boldsymbol{\nu}$) can be estimated from a measured channel using different high resolution algorithms [2] such as ESPIRIT (Es-

timation of Signal Parameters via Rotation Invariance), MUSIC (Multiple Signal Classification), MVM (Minimum Variance Method) and SAGE. In this work, the SAGE algorithm was used to extract the MPC parameters.

2.2.1 SAGE algorithm

SAGE algorithm [18] is one of the popular high resolution algorithm for estimation of the MPC parameters. The final output of the algorithm is a vector $\boldsymbol{\theta}_l$= [$\Omega_{t,l}$, $\Omega_{r,l}$, τ_l, ν_l, α_l] where the entries of the lth wave $\Omega_{t,l}$, $\Omega_{r,l}$, τ_l, ν_l, α_l are the AOD, AOA, delay, Doppler frequency and complex weight, respectively [1]. l is dependent on number of MPCs, and $l = [1 \dots L]$. The estimation algorithm can be divided into two steps: I. Initialization and II. Iteration.

In the initialization step the parameters are first estimated for the dominant multipath component and then other MPCs are estimated by employing a successive cancellation method [18].

$$y^{(l)}(t) = y(t) - \sum_{l'=1}^{l-1} s(t; \hat{\theta}_{l'}(0)). \tag{2.7}$$

In the iteration stage the values of $\boldsymbol{\theta}_l$ are re-estimated until convergence is reached or a certain number of iterations is completed. A flowchart of the SAGE algorithm [18] is given in Figure 2.1

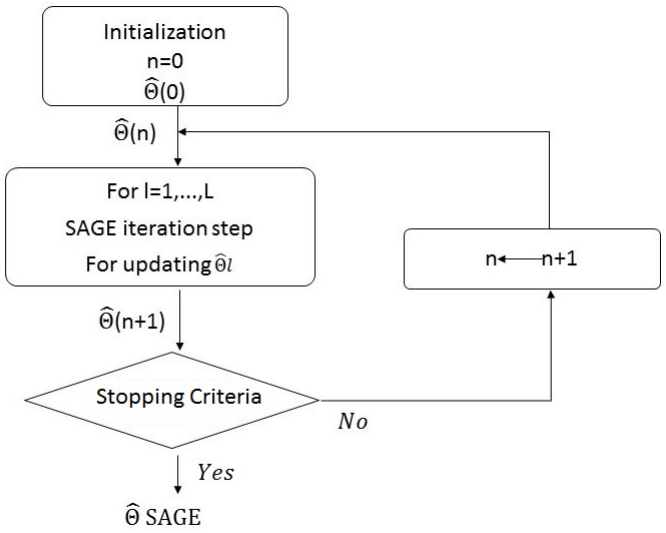

Figure 2.1: SAGE algorithm

[1]The reader should keep in mind that $\Omega_{t,l}$, $\Omega_{r,l}$ contains both azimuth and elevation angles.

In this work, the raw data obtained from the measurements consists of the transfer functions of the SIMO channels (between each single BS antenna element and all the antenna elements at the MS), which are used to get their corresponding impulse response estimates (IREs). To mitigate the effect of noise from channel IREs, multipath echoes are declared valid in a specific impulse-response-delay resolution interval only if the signal in that interval is at least 6 dB above the estimated noise in the IREs. Also, the IREs are subjected to a delay-gating filter, which was implemented by using a 700 m delay-window. This filter eliminates all multipath components that are 700 m in excess of the Tx-Rx separation. Then, SAGE was applied to each IRE in order to extract the AOA (both azimuth and elevation), complex amplitude, and delay of each multipath component.

2.2.2 Reconstruction of the MIMO channel incorporating parameters estimated from SAGE

As mentioned, Only $\Omega_{r,l}$, τ_l and α_l was estimated using SAGE algorithm. These parameters were used to reconstruct the channel matrix. The narrowband equivalent representation of the elements of the $\mathbf{H}$ matrix of Equation (2.5) (for a given frequency f) can be written as:

$$h_{n,m} = \sum_{l=1}^{L} g_{r(n)}(\Omega_{r(l,m)})\alpha_{l,m}e^{j2\pi f\tau_{l,m}}. \tag{2.8}$$

To take into account the effect of different frequencies, different values of f was used in Equation (2.8) and a shift in the AOA, i.e. $\Omega_{r,l}$ was used to consider different azimuthal orientation of the users.

2.3 Channel metrics

Evaluation of propagation-motivated channel metrics provide insight into the structure of the channel. It should be mentioned that most metrics cannot cover all aspects of the MIMO channel and some are dependent upon the used antenna pattern. In this work, a few channel metrics were studied to understand the spatial structure of the channel.

2.3.1 Channel Matrix Collinearity

The distance between two complex valued matrices having same dimensions can be calculated by [19]

$$c(\mathbf{H_0}, \mathbf{H_1}) = \frac{|Tr\{\mathbf{H_0}\mathbf{H_1^H}\}|}{||\mathbf{H_0}||_F||\mathbf{H_1}||_F}. \tag{2.9}$$

Here, $Tr\{.\}$, $(.)^H$, $||.||_F$ denotes the trace operator, hermitian transpose and Frobenius norm, respectively. This metric compares the similarity between the subspaces of the matrices under evaluation. In general, the collinearity describes how similar

the subspaces of the compared matrices are. This measure ranges between zero (no collinearity, i.e. matrices are orthogonal to each other) and one (full collinearity). A full collinearity between two channel matrices is encountered when [19]

- Both singular values and singular vectors are equal (i.e the channels are exactly equal).
- All singular values of individual matrices are equal.

2.3.2 Singular Value Spread

The singular value spread (Channel Conditon Number) of a channel matrix $\mathbf{H}$ can be described as a measure of orthogonality between the subchannels (i.e. individual user channels) [20]. The channel matrix $\mathbf{H}$ has a singular value decomposition

$$\mathbf{H} = \mathbf{U}\mathbf{\Sigma}\mathbf{V}^H, \tag{2.10}$$

where $\mathbf{U} \in \mathbb{C}^{M_R \times M_R}$ and $\mathbf{V} \in \mathbb{C}^{M_T \times M_T}$ are unitary matrices and $\mathbf{\Sigma} \in \mathbb{C}^{M_R \times M_T}$ is a diagonal matrix containing the singular values (σ) of the channel in an ordered manner, i.e $\sigma_1 \geq \sigma_2 \geq \cdots \geq \sigma_k$. The channel condition number (the singular value spread) κ is defined as

$$\kappa = \frac{\sigma_{\max}}{\sigma_{\min}}, \tag{2.11}$$

κ is bounded by the range $1 \leq \kappa \leq \infty$. Value of κ closer to 1 represents orthongonality between individual user channels and larger values represents difficulty in spatial separation.

2.3.3 Ratio of Condition Numbers

Another measure of channel similarity is given by the ratio of condition numbers [17]

$$\chi(\mathbf{H_0}, \mathbf{H_1}) = 10 \cdot \log_{10} \left(\frac{\sigma_{\max}(\mathbf{H_0})}{\sigma_{\min}(\mathbf{H_0})} / \frac{\sigma_{\max}(\mathbf{H_1})}{\sigma_{\min}(\mathbf{H_1})} \right), \tag{2.12}$$

where $\sigma_{\max}(\mathbf{H})$ and $\sigma_{\min}(\mathbf{H})$ denote the largest and smallest singular values of $\mathbf{H}$, respectively. With this metric, the channel similarity is denoted by the values close to 0 dB while any dissimilarity is denoted by the positive or negative values of χ.

Chapter 3

Measurement description

3.1 Measurement setup

As mentioned previously, this work was based on practical measurements. The measurements took place on the campus of Lund University, Lund, Sweden, in an area which can be best characterized as suburban environment. Both campaigns were carried out using the same measurement equipment, the RUSK-LUND channel sounder. In addition, in both campaigns, a cylindrical array with 128 elements was used at the receiver, and 8 transmit elements were used at the BS side. The sounding signal is conveyed to each of the remote BS's locations through the optical backbone network of the campus by means of radio-over-fiber (RoF) transceivers. Please refer to [21] for more details about the equipment used. The difference between the two campaigns was the configuration of the BS antenna elements: in setup-I the BS antenna elements formed a linear array with variable inter-patch spacing at one BS, and in setup-II the BS antenna elements were distributed at two BSs, each BS with 4 co-located antenna elements. More details are given in the sequel:

3.1.1 Measurement Equipment

The measurement campaign was carried out using the RUSK-LUND channel sounder at a center frequency of 2.6 GHz and a measurement bandwidth of 40 MHz [22]. At the BS side, four cross-polarized patch antennas were used. The arrangement of the BS antennas is different in setup-I and setup-II as will be explained later. The signal broadcasted by the BS is received by the receiver [1] equipped with 64 cross-polarized antenna elements in a stacked uniform cylindrical array configuration (Figure 3.1.a.). The cylindrical array consists of four rings each of which has 16 cross-polarized antenna elements. The transmit-receive

[1] In this work, three distinct terms have been used. Receiver: It refers to the cylindrical array that was used in the measurement campaign. MS Unit: Two vertically adjacent patches from the receiver was considered as a MS unit. Thus each MS unit has four antenna elements. User: Users were assumed to have two antenna elements, i.e. a subset of elements from the MS unit. The users can have one antenna element (MU-MISO) or two antenna elements (MU-MIMO). The MS unit and user will be further explained in section 3.2.2

channels are sounded in a time-multiplexed fashion such that all of the receive antenna elements are polled in succession prior to switching to the next transmit antenna element, where a 6.4 μs sounding signal is used. The data resulting from this sounding operation is referred to as a snapshot, consisting of 1024 wide-band transmit-receive channels (128 receiver antenna elements $\times$ 8 BS antenna elements), each of which has 257 frequency bins. A distance wheel is used to trigger the acquisition of the MIMO snapshots every λ movement (approximately 11 cm), and $\lambda/2$ movement (approximately 6 cm) in setup-I and setup-II, respectively. The measured snapshots are used to extract the MIMO user channels as described in the next section.

Figure 3.1: Antennas at the receiver and at the BS. (a) receiver antenna: stacked uniform cylindrical array with 64 cross-polarized antenna elements arranged in four rings. (b) BS antennas: co-located arrangement used in setup-II with inter-patch spacing of $\lambda/2$ (back view). (c) BS antennas: mounted on a tripod to facilitate adjusting the inter-patch spacing for setup-I, the photo is with inter-patch spacing of 1 m (back view).

3.1.2 Setup-I

In setup-I, only one BS, placed on the rooftop of a four story building (E-building) in an equally-spaced linear configuration is used. The BS is equipped with four

cross-polarized antennas, i.e. four patches each of which has two antenna elements. The patch antennas are mounted on a tripod to facilitate adjusting the inter-patch spacing, which is defined as the distance between two adjacent patch antennas; see Figure 3.1.c. The inter-patch spacing is varied to the following 8 values: $\lambda/2$, λ, 0.25 m, 1 m, 2 m, 4 m, and 8 m corresponding to a BS antenna array aperture from 0.17 m to 24 m. The measurement scenarios include both LOS and NLOS propagation conditions. For each inter-patch spacing value, the receiver is moved (at around 0.5 m/s) on three routes: Route 1 is mainly LOS, and Routes 2 and 3 are mainly NLOS. In the measurement area, there are only few buildings; however, the main interacting objects are leafy trees. Therefore, the propagation conditions for the measurement routes may alter from LOS to NLOS, or vice versa, due to the sudden appearance or disappearance of heavy branches between the receiver and the BS, see Figure 3.2. A distance wheel was used to trigger the acquisition of MIMO snapshots every λ movement, which resulted in collecting 350 snapshots per route. The details of this measurement campaign can be found in [15],[22].

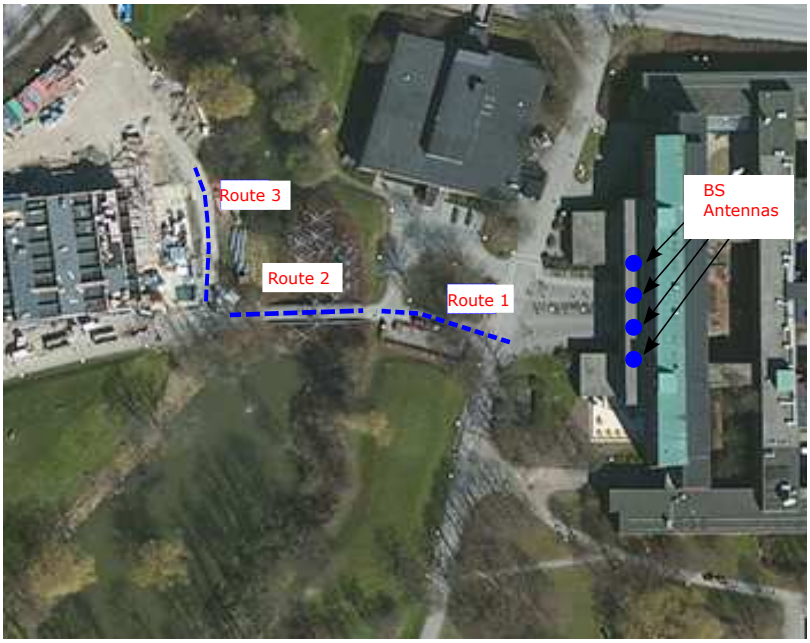

Figure 3.2: Aerial photo of the measurement area illustrating setup-I. BS antennas are indicated with the blue circles all placed at one BS. The receiver measurement routes are plotted in dashed blue lines: Route 1 is mainly LOS; Route 2 and Route 3 are mainly NLOS.

3.1.3 Setup-II

In setup-II, the BS antennas are distributed at two BS sites. Each BS was equipped with two cross-polarized antenna patches, i.e. four closely-located antenna ports. Figure 3.1.b. illustrates an example of the antenna arrangement at each BS site, where the distance between adjacent antenna patches is fixed at half wavelength. One BS was placed out of a window in the third floor of the E-building while the other BS was placed outside of a window in the second floor of the studiecentrum, hereon, referred to as BS-E and BS-S, respectively. This arrangement results in a distance of 60 m between the two BSs. The receiver was moved on five different routes in the surrounding area, each of them having a length of approximately 25 m. The distance wheel was adjusted to acquire MIMO snapshots every $\lambda/2$ movement of the receiver, resulting in 450 snapshots per route. The map of setup-II is shown in Figure 3.3; the movement of the receiver covered most of the walking paths as indicated by the red dots.

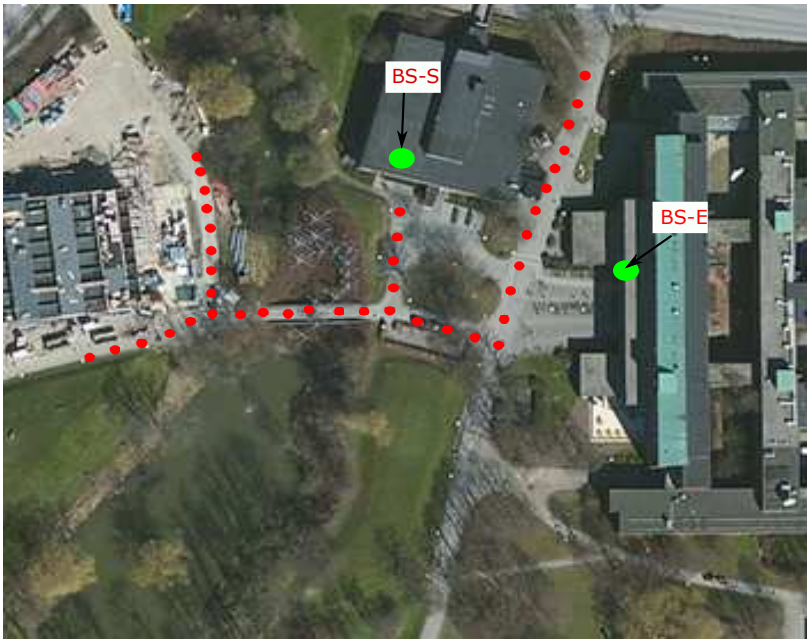

Figure 3.3: Aerial photo of the measurement area illustrating setup-II. BS-E and BS-S are indicated with the large green circles. Each BS is equipped with co-located antenna arranged as depicted in 3.1.b. The receiver measurement route is indicated by the small red circles.

3.2 Extracting MIMO user channels in setup I

Each measured snapshot has a size of 128 receiver elements x 8 BS elements x 257 frequency bins. For this work, only a subset of receiver antenna elements was chosen to construct the user channels assuming that users have random orientation. Also, four BS antennas were chosen at each instance and hence, the number of users were restricted to four; resulting in: a 4×4 MISO channel (when users were assumed to have only one antenna element), and an 8×4 MIMO channel (when users were assumed to have two antenna elements). While the MU-MIMO channel was evaluated, the worst case scenario in terms of users' orientation and frequency was considered, where the users were chosen such that they have same orientation and use same frequency.

3.2.1 Antenna setup and selection at the BS

In setup-I, along with the effect of antenna polarization, the effect of BS antenna array aperture was studied. The schematic diagram of setup-I is given in Figure 3.4

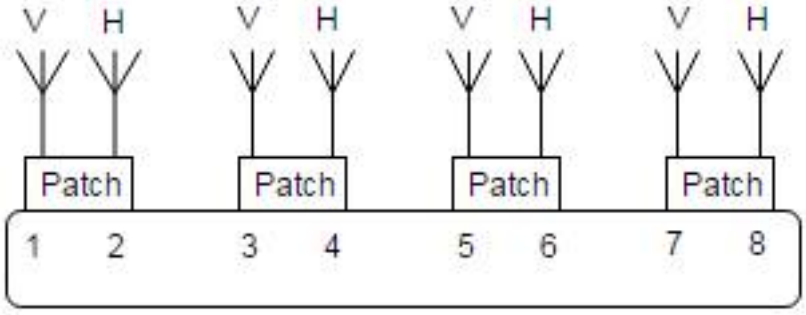

Figure 3.4: Schematic diagram of BS (Setup-I)

For a fair comparison between single polarized and cross-polarized configurations, not all BS antennas were considered at once. Rather, separate configurations were chosen for BS antennas (each of which has only 4 selected antenna elements) and sum-rate capacities were found based on these configurations and compared subsequently. Below, different configurations for setup-I are clarified.

Vertical polarization (V.Pol.)

Here, antenna element no. 1, 3, 5, 7 i.e. all vertically polarized antenna elements were chosen. The choice of these elements ensured that all antenna elements at the BS side would have the same inter element distance.

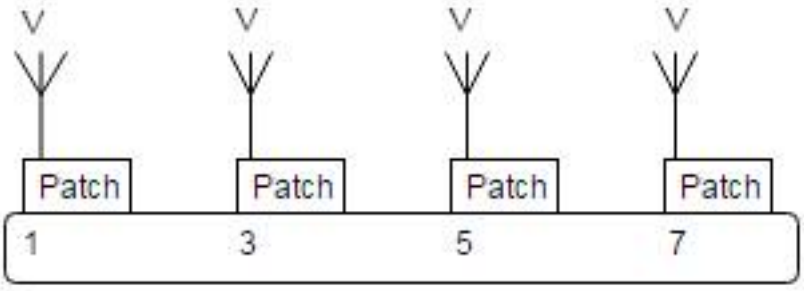

Figure 3.5: Schematic diagram of BS elements Vertical polarization (V.Pol.)

Horizontal Polarization (H.Pol.)

Here, antenna element no. 2, 4, 6, 8, i.e. all horizontally polarized antenna elements were selected. The selection of these antenna elements ensured the completeness of selection of single polarized BS configuration.

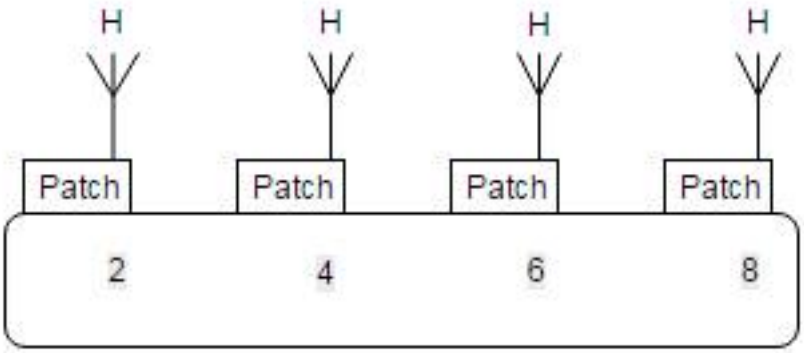

Figure 3.6: Schematic diagram of BS elements Horizontal Polarization (H.Pol.)

Cross polarization-I (Co.Pol.I)

In Co.Pol.I, antenna element no. 1, 4, 5, 8 i.e. equally separated cross polarized elements were selected. This configuration incorporates both spatial and polarization separation.

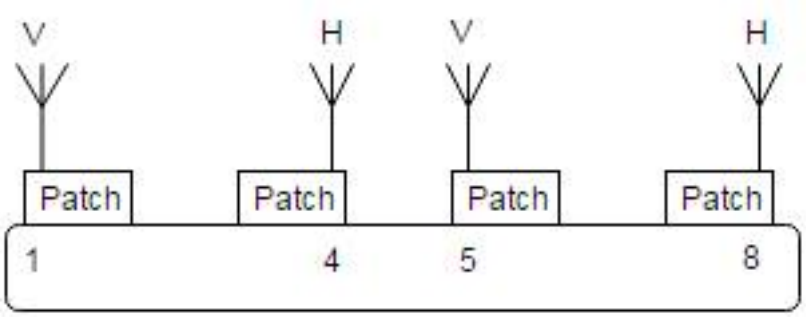

Figure 3.7: Schematic diagram of BS elements Cross polarization-I (Co.Pol.I)

Cross polarization-II (Co.Pol.II)

In Co.Pol.II, antenna element no. 1, 2, 7, 8 were selected, i.e. one vertical and one horizontal element spaced close together ($\lambda/2$) but the sets of cross-polarized elements were spaced apart from each other. This configuration was chosen in order to be able to compare the sum-rate capacity performance of Cross polarization-II with that of Cross polarization-I. The result can motivate the use of four or two patches.

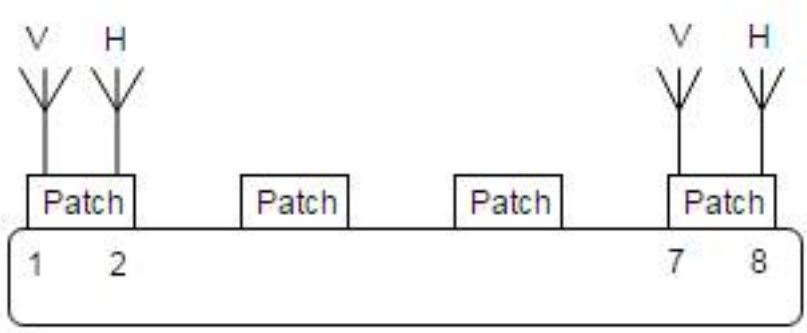

Figure 3.8: Schematic diagram of BS elements Cross polarization-II (Co.Pol.II)

Schematic diagrams of the configurations can be found in figures 3.5-3.8.

3.2.2 Antenna setup and selection at the MS

The users were chosen such that they were always 5λ apart from each other. Each two cross-polarized vertically adjacent (with a $\lambda/2$ vertical spacing) patch antennas from the receiver uniform cylindrical array (see Figure 3.1.a) are considered to represent a MS unit. Thus each MS unit has 4 antenna elements, 1, 2, 3 and

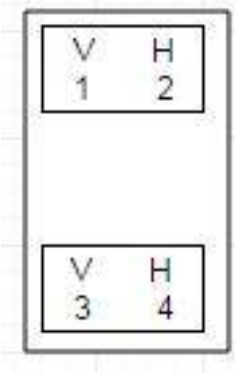

Figure 3.9: Schematic diagram of Mobile station antennas

4 and the distance between any of these antennas is always $\lambda/2$. Figure 3.9 represents the schematic diagram of a single MS unit. To keep resemblance with reality, a user was always presumed to have cross polarized antennas when the user has multiple antennas. As a result, two different possibilities arose, e.g. one can choose MS unit element set 1, 4 or 2, 3 to represent a user. Hence, both possibilities were evaluated individually to find the sum-rate capacity, and the sum-rate results were averaged over. When we considered one antenna element at the user, this antenna element was chosen randomly, such that there is 50% probability of having vertical or horizontal polarization.

3.3 Extracting MIMO user channels in setup-IIA

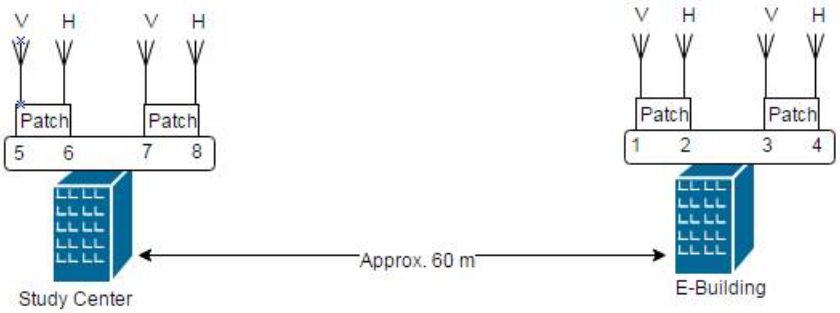

Figure 3.10: Schematic diagram of BS (for both Setup-IIA and SetupII-B)

In setup-II, the individual BS antenna array aperture was fixed, so only the effect of antenna polarization on the sum-rate capacity was studied. The BS antenna elements were chosen according to six different configurations. However, two different approaches were followed in analyzing measurement data of setup-II

and these would be termed as setup-IIA and setup-IIB in the rest of this paper. The difference between them is at the user side; setup-IIB incorporates measured Plannar Inverted F Antenna (PIFA) patterns (including the effect of user body and posture), whereas setup-IIA uses the data obtained from the campaign directly. Figure 3.10 shows the schematic diagram of setup-II (A, B).
Similar to setup-I, four BS antennas were selected at each instance and each of the four selected users were assumed to have two antenna elements, resulting in an 8×4 MIMO channel.

3.3.1 Antenna setup and selection at the BSs

Antenna selections at the BS side resulted in three different configurations, namely, Horizontal polarization, Vertical polarization and Cross Polarization. The selection of the antenna element is described below:

Horizontal Polarization (H.Pol.)

Here, antenna elements 2, 4 from BS-E and 6, 8 from BS-S; i.e. horizontal antenna elements were selected.

Vertical Polarization (V.Pol.)

To study yet another single polarized configuration, antenna elements 1, 3 from BS-E and 5, 7 from BS-S; i.e. vertical antenna elements were selected. Performance of H.Pol. and V.pol. configurations, in terms of sum-rate capacity were taken as the reference for the cross-polarized performances.

Cross polarization-I

Here, antenna elements 1, 4 from BS-E and 5, 8 from BS-S; i.e. cross-polarized elements were selected.

Cross polarization-II

In Cross polarization-II configuration, antenna elements 2, 3 from BS-E and 6, 7 from BS-S; i.e. cross-polarized elements were selected.

Cross polarization-III

In Cross polarization-III configuration, antenna elements 1, 4 from BS-E and 6, 7 from BS-S; i.e. cross-polarized elements were selected.

Cross polarization-IV

Here, antenna elements 2, 3 from BS-E and 5, 8 from BS-S; i.e. cross-polarized elements were selected.

Since Cross polarization I to IV are equivalent in polarization, they were averaged to calculate final results of the cross-polarized antenna configuration (hereon referred to as Co.Pol.). The motivation was to have a greater statistical accuracy.

3.3.2 Antenna setup and selection at the MS

The receiver side antennas were chosen similar to setup-I in section 3.2.2.

3.4 Extracting MIMO user channels in setup-IIB

As mentioned before, Setup-IIA and Setup-IIB has same BS antenna configurations. In the latter approach, the effect of the BS antenna polarization with the effect of the body included in the user antenna pattern, is studied. Since the user with the antenna are considered as one radiating unit, i.e. one large-antenna, the choice of the user holding the device in different positions affects the MIMO channel characteristics. Thus, for setup-IIB composite channel method [16] was used for analysis. The MPC parameters (e.g. delay, AOA, complex gain) were extracted using SAGE algorithm described in section 2.2. These parameters were combined with custom user antenna patterns to create new channel matrices **H**. The MS unit had two cross polarized receive antenna patches and the user was assumed to hold the MS unit in two different modes, namely; talk mode and browse mode. Each user configuration has distinct impact on efficiency loss due to absorption by hand and body. For the talk mode, the handset was placed in three positions inside the hand with 2 cm difference between each position. These three positions are referred to as TM1, TM2 and TM3, respectively. While for the browse mode, the difference between each position is in terms of angles of holding the handset and they are referred to as DM1, DM2 and DM3, respectively. As can be seen in Figure 3.11 the device had four elements, but in this work only two of them (element 1 and 2) were used, resulting yet again in an 8×4 MIMO channel.

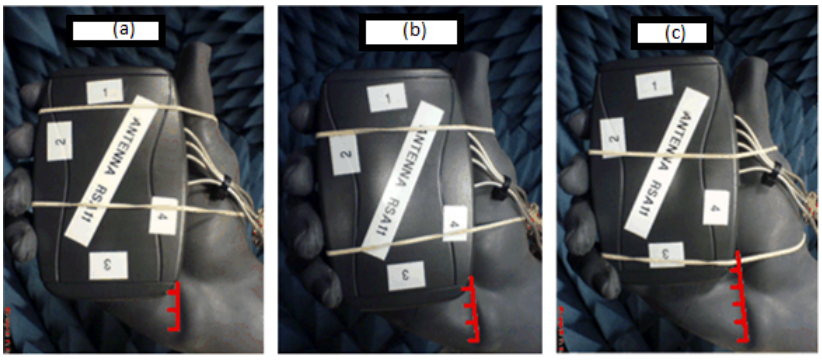

Figure 3.11: Handset positions in hand (a) Position1, (b) Position 2, (c) Position 3. 1, 2, 3, 4 represents the element numbers (Talk mode)

Talk Mode

In talk mode the user was assumed to hold the phone close to the air (normal call on cell phone). Since each user holds the phone in a different way, three different talk mode measurements were performed. The sum-rate capacity results from these three measurements were averaged over to yield a more realistic representation of the real world. Figure 3.12 shows the polar plot of vertical gain of antenna 1 of position TM2. In Figure 3.13 the 2D patterns for talk mode are shown where the slice is taken at $\theta = 90°$.

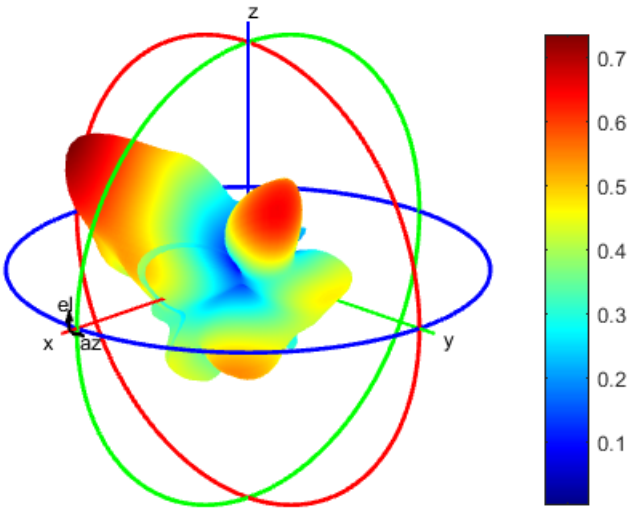

Figure 3.12: Radiation pattern of antenna element 1 of position TM2 (vertical gain in Talk Mode)

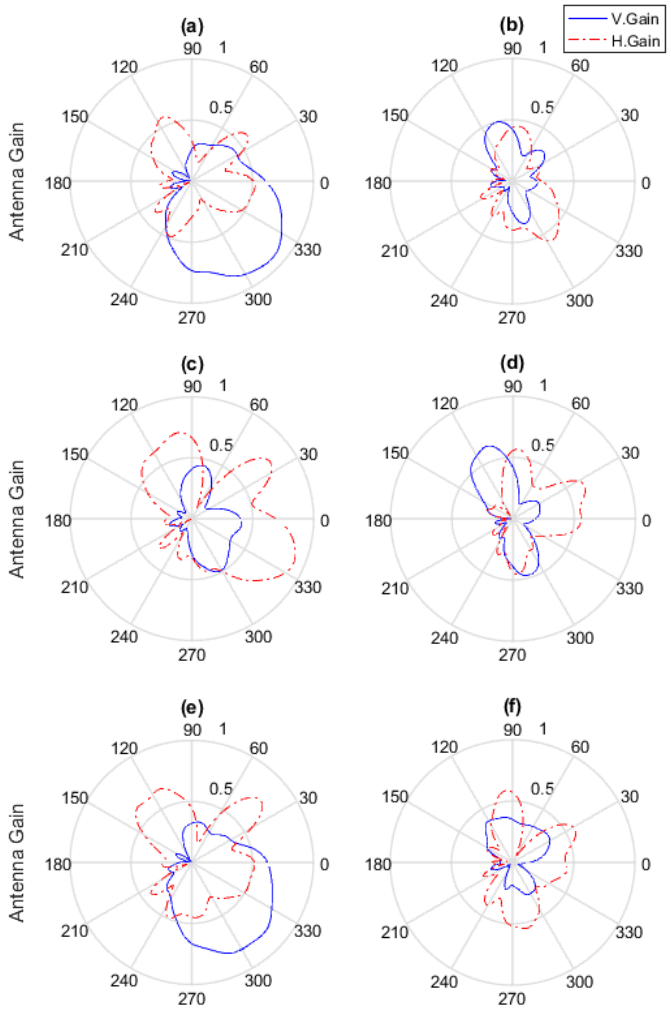

Figure 3.13: Radiation pattern for all elements. (a) Element 1, TM1, (b) Element 2, TM1, (c) Element 1, TM2, (d) Element 2, TM2, (e) Element 1, TM3, (f) Element 2, TM3

Browse Mode

In the browse mode the user was assumed to hold the phone close to the lap (in front of chest cavity) and that the user holds the phone in three different angles. Three different measurement were taken in order to yield a better representation of the real world. As in talk mode, the sum-rate capacity results were also averaged over. Figure 3.14 shows the polar plot of vertical gain of antenna element 1 of position DM2. In Figure 3.15 the 2D patterns for browse mode is shown where the cut is taken at $\theta = 90°$.

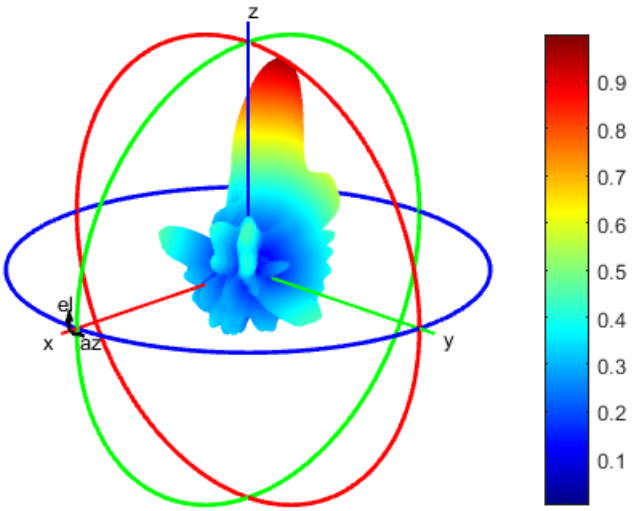

Figure 3.14: Radiation pattern of antenna element 1 of position DM2 (vertical gain in Browse Mode)

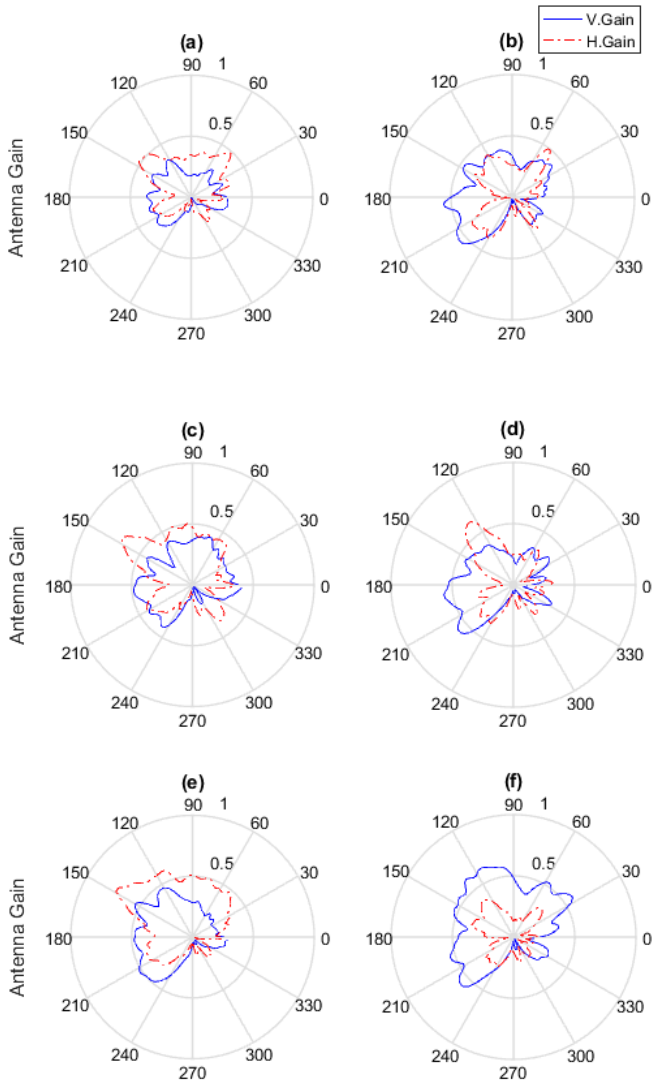

Figure 3.15: Radiation pattern for all elements. (a) Element 1, DM1, (b) Element 2, DM1, (c) Element 1, DM2, (d) Element 2, DM2, (e) Element 1, DM3, (f) Element 2, DM3

As can be seen from Figure 3.13 and 3.15 the antenna radiation pattern depends not only on the elements chosen, but also on posture and position of the device in the users' hand.

Chapter 4

MU-MIMO BC capacity

4.1 Signal model

In a narrow-band time-invariant wireless channel with M_T transmit antennas and K users each with M_R=1 antenna, the MIMO BC channel can be modelled as follows [1]:

$$\mathbf{Y} = \mathbf{H}\mathbf{x} + \mathbf{n}. \tag{4.1}$$

Here $\mathbf{Y} = [y_1, y_2, y_3.....,y_k]^T$ is a $K \times 1$ vector where each element of $\mathbf{Y}$ represents the received signal by a user. $\mathbf{x} = [x_1, x_2, x_3.....,x_k]^T$ is a $M_T \times 1$ vector where each element represents the transmitted signal from the BS. $\mathbf{H} \in \mathbb{C}^{K \times M_T}$ represents the channel matrix. In this work, it is assumed that the channel matrix is known at the BS. The total power constraint on the signals from transmit antennas is $\sum_{k=1}^{K} P_k = P$, where P is the total transmit power and is equally allocated amongst the users. P_k is the power allocated to the kth user. Furthermore, $\mathbf{n} = [n_1, n_2, n_3.....,n_k]^T$ is a $K \times 1$ vector that represents Gaussian noise, $\mathbf{n} \sim \mathbb{C}\mathcal{N}(0,N_o\mathbf{I_{M_R}})$ with zero mean and N_o variance.
It should be noted that the variable dimensions of Equation (4.1) would change if each user had multiple receive antennas. With each user having M_R receive antennas, the variables $\mathbf{Y}$,$\mathbf{H}$ and $\mathbf{n}$ in Equation (4.1) would have the dimensions of (K $\cdot M_R$)$\times$1, (K$\cdot M_R$) $\times$ M_T and (K$\cdot M_R$)$\times$1, respectively.

4.2 Capacity calculation

The achievable capacity region for MIMO broadcast channels is still an open problem [1]. A set of achievable capacity region was published first by Caire and Shamai [23] by using Dirty Paper Coding (DPC) concepts by Costa [24]. A duality between the achievable rate region of BC channels and multiple access capacity region was published by Vishwanath et Al [25]. From the work of Yu and Cioffi [26] the achievable rate region of MIMO BC was mentioned as [1]

$$C_{BC} = \min_{\mathbf{R_{nn}}>0,[\mathbf{R_{nn}}]_{k,k}=N_o} \max_{Tr(\mathbf{R_{xx}})=P} \log_2 \frac{det\left(\mathbf{H}\mathbf{R_{xx}}\mathbf{H}^H + \mathbf{R_{nn}}\right)}{det\left(\mathbf{R_{nn}}\right)}, \tag{4.2}$$

where $\mathbf{R_{nn}} = \mathcal{E}\{nn^H\}$ and $\mathbf{R_{xx}} = \mathcal{E}\{xx^H\}$ and $\mathcal{E}$ represents expectation operator. However, this capacity region is achievable through DPC which is a non-linear precoding scheme and cumbersome to implement in practical systems. Thus, less optimal yet easy to implement linear precoding schemes are frequently used in practical systems. In this thesis, Zero Forcing precoding and MMSE precoding techniques were used to evaluate the sum-rate capacity of the MIMO channel.

4.3 Linear precoding techniques

Let us return to our signal model in section 4.1, $\mathbf{x}$ in the signal model of Equation (4.1) is the transmitted signal vector from the BS. If we consider the actual data stream for the user k as S_k, then $\mathbf{x} = \mathbf{WS}$, where $\mathbf{W} = [\mathbf{w_1}, \mathbf{w_2}, \mathbf{w_3}....., \mathbf{w_k}]^T$ is the $M_T \times M_R$ precoding vector applied by the BS. If we consider single antenna users then the sum-rate capacity can be written as [13]

$$C_{BC} = \sum_{k=1}^{K} \log_2 (1 + \rho_k). \tag{4.3}$$

In Equation (4.3), ρ_k is the SINR for user k. It can be calculated as-

$$\rho_k = \frac{\left|\mathbf{H}^{(k)}\mathbf{w_k}\right|^2}{N_o + \sum_{i \neq k} \left|\mathbf{H}^{(k)}\mathbf{w_i}\right|^2}, \tag{4.4}$$

where $\mathbf{H}^{(k)}$ and $\mathbf{w_k}$ are the channel and beamformer in the BS side for the kth user, respectively. $\mathbf{W}$ is a general precoder matrix that can be designed according to design criteria. As mentioned, in this work, the ZF and MMSE precoding techniques are investigated.
Although Equations (4.3) and (4.4) are still valid even if the user has multiple antennas, this arrangement imposes over-constraints on the precoding schemes. In that context, the constraint of using aforementioned equations is that the total number of Rx antennas have to be less than or equal to the total number of Tx antennas, i.e. $M_R \leq M_T$. The transmitter essentially treats each receiving antenna as a separate user and this restricts the performance in terms of capacity. Block Diagonalization (BD) is a technique that improves the performance [27], although the limitation on the total number of receive antennas still remains in this scheme. Furthermore, the BD scheme assumes that the total number of data streams for a user is equal to the number of Rx antennas of that user, i.e. multiplexing of data is presumed. Coordinated beamforming technique [1], however, removes these constraints and with optimized power allocation techniques, maximizes the capacity [28]. In coordinated-beamforming technique, both BS and user implement beamforming and the SINR equation of (4.4) is modified to:

[1] Not to be confused with the CS/CB techniques; CS/CB is a different CoMP strategy, whereas Coordinated beamforming in this section and following sections context is a beamforming method used for CoMP systems using JT/JP strategy.

$$\rho_k = \frac{\left|\mathbf{u_k}^H \mathbf{H}^{(k)} \mathbf{w_k}\right|^2}{N_o + \sum_{i \neq k} \left|\mathbf{u_k}^H \mathbf{H}^{(k)} \mathbf{w_i}\right|^2}. \tag{4.5}$$

Here $\mathbf{u_k}$ is the $N_r \times 1$ beamformer applied by the kth user and $\mathbf{u_k}^H$ is the Hermitian transpose of $\mathbf{u_k}$.

4.3.1 Zero Forcing Precoding

In Zero Forcing linear precoding technique [1], the intent is to transmit the user signal to the desired user and nulls steered towards the other users. In this case the ith column of the zero Forcing precoding matrix $\mathbf{W}_{ZF,i}$ can be calculated as-

$$\mathbf{W}_{ZF,i} = \frac{\mathbf{h_i}^{(\dagger)}}{\sqrt{\left|\left|\mathbf{h_i}^{(\dagger)}\right|\right|_F}}. \tag{4.6}$$

Where $\mathbf{h_i}^{(\dagger)}$ is the ith column of $\mathbf{H}^H \left(\mathbf{H}\mathbf{H}^H\right)^{-1}$ and appropriate power constraints can be chosen. $||.||_F$ denotes the Frobenius norm. Depending on the channel condition, some users will receive little amount of power, rendering ZF a suboptimal precoding technique. This behavior is especially prevalent in low SNR region and ill conditioned channels.

4.3.2 MMSE Precoding

To alleviate the problem inflicted by ZF precoding, MMSE precoding can be used as an alternative technique. The MMSE precoding matrix can be designed as [29]

$$\mathbf{W}_{MMSE} = \mathbf{H}^H \left(\mathbf{H}\mathbf{H}^H + \beta \mathbf{I}\right)^{-1}. \tag{4.7}$$

Here β is called the regularization factor. If $\beta = 0$, then MMSE precoding reduces to ZF precoding. In practice, regularization factor is chosen as $\beta = \frac{M\sigma^2}{P}$, where M, P and σ^2 are the number of Tx antennas, total transmit power and noise variance, respectively. Choice of β approximately maximizes the SINR at each receiver [29]. The performance of MMSE technique is superior to that of ZF at low SNR region while at high SNR, capacity evaluated (performance) from both precoding techniques converges. However, power allocation techniques in MMSE precoding are not straightforward [29].

4.3.3 Coordinated beamforming

As mentioned in section 4.3 , coordinated beamforming removes the limitations that are inherent in BD technique. The constraint on the coordinated beamforming is that the total number of users have to be equal to the number of transmit

antennas at the BS, i.e. $M_T = K$. Since each user can be equipped with multiple antennas, then the total number of Rx antennas can be greater than the total number of transmit antennas, i.e. $M_R > M_T$ can be supported by coordinated beamforming technique. Furthermore, data streams for each user can be used in multiplexed mode or advantage of antenna diversity can be gained for each user. The complexity of this method can be considered as a drawback as it requires coordination between the user and the BS. The beamformers are finalized after a few iterations making it somewhat unstable in scenarios where the user is moving fast. In [28], general ideas regarding coordinated beamforming along with two algorithms about coordinated zero forcing and general coordinated beamforming has been discussed. The general coordinated beamforming algorithm [28], is used in this thesis work and is given here for a complete description purpose only.

Table 4.1: Algorithm for general coordinated beamforming

1) Assume an initial set of $\mathbf{u_1}$.....$\mathbf{u_k}$. One good candidate is to use the dominant left singular vectors of individual channel matrices $\mathbf{H_j}$.
2) Given $\mathbf{u_1}$.....$\mathbf{u_k}$, calculate $\overline{\mathbf{H}}$ and find $\mathbf{W}$ using MMSE or any optimal beamforming.
3) Given $\mathbf{W}$, recalculate the receiver beamformers $\mathbf{u_1}$.....$\mathbf{u_k}$ according to some assumed receiver design (MMSE,MRC etc).
4) If the SNR or sum rate achieved by $\mathbf{W}$ and $\mathbf{u_j}$ has changed from last iteration, go to step 2; otherwise, stop.

To calculate the user side beamforming in step 3 of table 4.1, the MMSE beamformer from [13] was used. The user side beamformer equation is:

$$\mathbf{u_k} = \mathbf{u_o} \left[\mathbf{I} + \sum_{i \neq k} \mathbf{H}^{(k)} \mathbf{w_i} \mathbf{w_i}^H \mathbf{H}^{(k)^H} \right]^{-1} \mathbf{H}^{(k)} \mathbf{w_k}. \tag{4.8}$$

Here $\mathbf{u_k}$ and $\mathbf{w_k}$ are receive and transmit beamformers for kth user, respectively. $\mathbf{H}^{(k)}$ represents the channel for kth user and $\mathbf{u_o}$ is chosen such that the vector $\mathbf{u_k}$ has unit norm.

Chapter 5

Results and analysis

5.1 Setup-I: Single BS with variable aperture

The measurements were taken as described in section 3.1.2 and the results were saved as a channel matrix $\mathbf{H}$. The dimensions of the recorded matrix were $4 \times 8 \times 32 \times 20 \times 350$ where the dimensions refer to MS antenna elements (4), BS antenna elements (8), different azimuth orientations (32), frequency bins (20) and snapshots (350). Then the channel matrices were extracted according to the antenna configurations described in section 3.2. Normalization was performed on each extracted channel matrix as explained in the sequel.

5.1.1 Normalization

It is important to normalize the channel matrices to interpret the results correctly. Thus the normalization method has to be adapted according to the analysis scenario and assumptions. In this work, each snapshot was normalized based on the neighboring 8 snapshots (including itself, total 9 snapshots). For instance, when snapshot 5 was taken, snapshots 1 to 9 were considered in the normalization process. And then other snapshots were considered as a moving average window. So, for one instance the normalization formula was-

$$\mathbf{H}_{norm}^{(n,s,l)} = \mathbf{H}^{(n,s,l)} \left[\frac{1}{L \times S \times N \times M_T \times M_R} \sum_{l=1}^{L} \sum_{s=1}^{S} \sum_{n=1}^{N} \left|\left| \mathbf{H}^{(n,s,l)} \right|\right|_F^2 \right]^{-1/2}. \quad (5.1)$$

Where $L = 32$, $S = 9$, $N = 20$, $M_T = 4$, and $M_R = 2$ are the no. of azimuth orientations, no. of snapshots taken for averaging, frequency bins, no. of BS and user antennas, respectively. With this normalization method, the difference in power between different patches, frequencies and snapshots within a distance of 1 m was preserved. It was assumed that the BS has a power scheduler that can compensate for large scale fading and path loss within 1 m.

5.1.2 Results and analysis

As described earlier, four BS antenna elements with different polarization setups and four users with 0.5 m inter-user spacing were evaluated. The users have

the same azimuth orientation. Furthermore, users can have one antenna element (MU-MISO) or two antenna elements (MU-MIMO). Results for MU-MISO and MU-MIMO are shown below.

MU-MISO

As a simple case of MIMO, users with one antenna element, where polarization of the antenna of each user was randomly selected, were considered to study the sum-rate capacity behavior with respect to the distance between BS antenna elements.

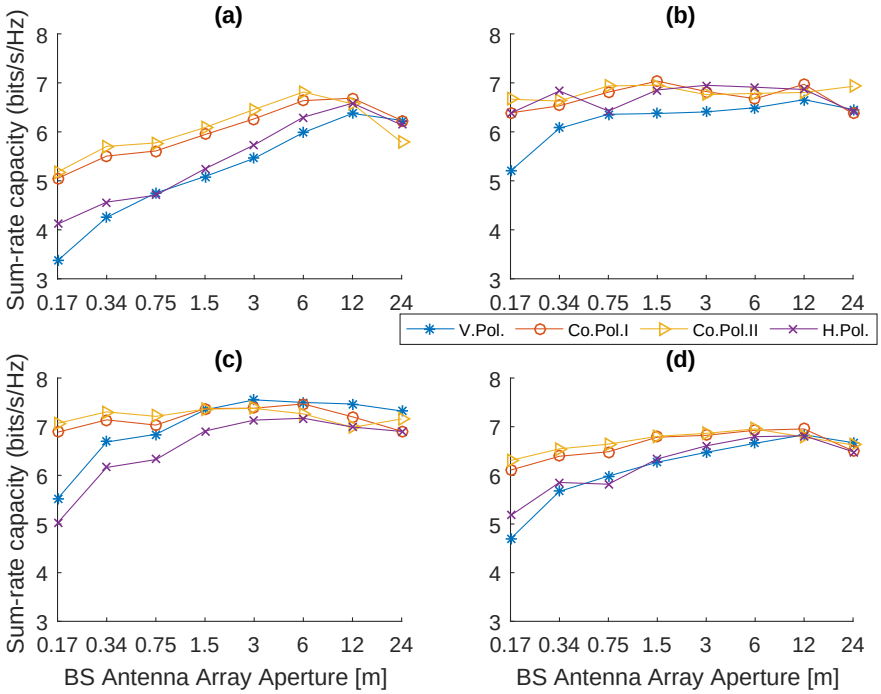

Figure 5.1: Ergodic sum-rate capacities using MMSE beamformer for different BS antenna array aperture: a) Route 1, b) Route 2, c) Route 3, d) All Routes

In Figure 5.1 the ergodic sum-rate capacity of users with one antenna element and using MMSE beamformer at the BS have been presented. Each route was analyzed separately and also sum-rate capacity of all routes combined is depicted to show a complete analysis. It can be observed that in route 1 (which is mostly LOS) the overall sum-rate capacity for all scenarios are the least which increases in route 2 (a mix of LOS and NLOS) and the most in route 3 (mostly NLOS scenario). Considering the overall scenario, we can draw a few conclusions:

- For vertically polarized BS antennas, 48% sum-rate capacity improvement

is observed when the array size is changed from 0.17 m to 12 m.

- For cross-polarized BS antennas, only 14% sum-rate capacity improvement is observed when the total array size varies from 0.17 m to 12 m.

- The difference in sum-rate capacity between vertically polarized and cross-polarized antennas is largest when the array size is 0.17 m, about 34% improvement when cross-polarized antennas are used. This difference diminishes when the array size reaches 12 m..

- For cross-polarized BS antennas, when the array size is 1.5 m and above, there is no difference in sum-rate capacity between Co.pol.I and Co.Pol.II. This indicates that two cross-polarized patches instead of four single polarized patches can be used at the BS.

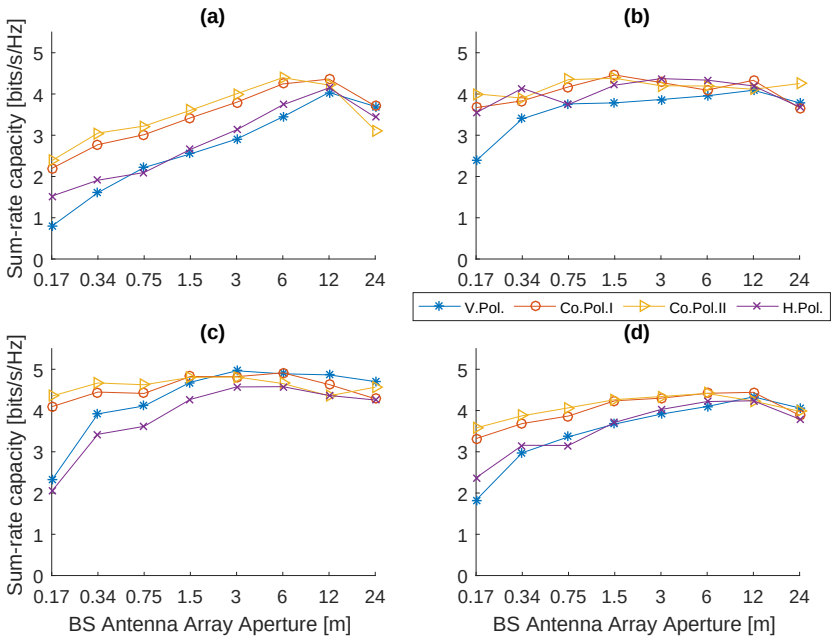

Figure 5.2: Ergodic sum-rate capacities using ZF beamformer for different BS antenna array aperture: a) Route 1, b) Route 2, c) Route 3, d) All Routes

Figure 5.2 depicts the ergodic sum-rate capacity of users with one antenna element and using ZF beamformer at the BS. Comparing Figures 5.1 and 5.2 it was found that MMSE gives 57% increase in the total sum-rate capacity which is also congruent with the theory [1].

MU-MIMO

For complete analysis of true MU-MIMO, users with multiple antennas were considered. As mentioned previously, only cross-polarized antenna elements at the user side were investigated. Using the observations of MU-MISO, regarding ZF and MMSE beamformer, the analysis was restricted to the use of MMSE equalizer at the user side. Also as mentioned in section 4.3.3, general coordinated beamforming algorithm was used for the overall analysis.
Similar results as MU-MISO can be concluded from Figure 5.3 regarding sum-rate capacity:

- The improvement in ergodic sum-rate capacity is largest between vertical and cross-polarized antenna configurations when BS array size of 0.17 m, about 72% improvement when cross-polarized antennas are used. With increasing the BS array size, SRC increases monotonically to certain point but eventually saturates when the array size reaches 12 m and the difference in the sum-rate capacity among different antenna polarizations becomes negligible.
- The SRC increases by 60% when the BS array size changes from 0.17 m to 12 m for vertically polarized BS elements. For cross-polarized elements the improvement is only 19%.

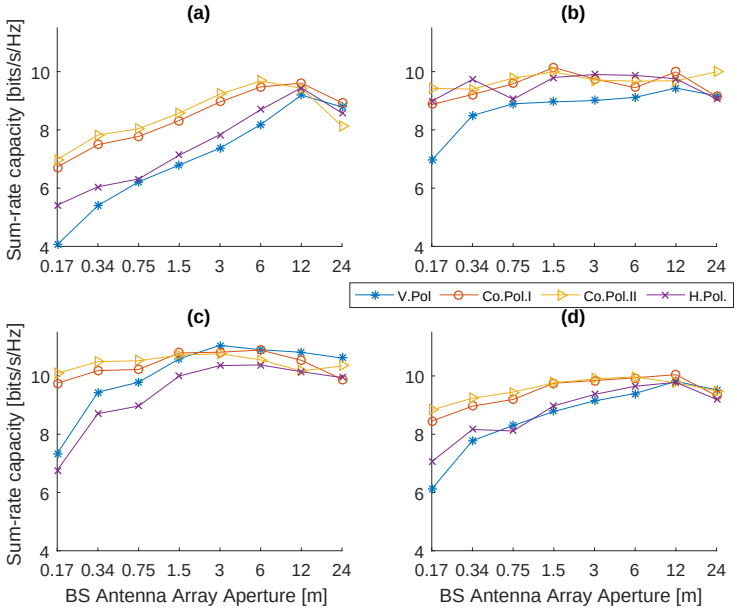

Figure 5.3: Ergodic sum-rate capacities using general coordinated beamforming for different BS array aperture: a) Route 1, b) Route 2, c) Route 3, d) All Routes

For both MU-MISO and MU-MIMO a few common observations can be made:

- There is a significant difference in sum-rate capacity between the single polarized and cross-polarized configurations when the BS antenna aperture is 0.17 m.
- When the BS antenna array aperture is 1.5 m, the capacities for Co.Pol.I and Co.Pol.II are close. This is true for V.Pol. and H.Pol configurations as well. But there is a significant difference between these two sets of sum-rate capacities.
- With increasing the BS antenna array aperture, the sum rate capacities increase monotonically but saturates at 12 m and the difference between the single- and cross-polarized configurations diminishes.

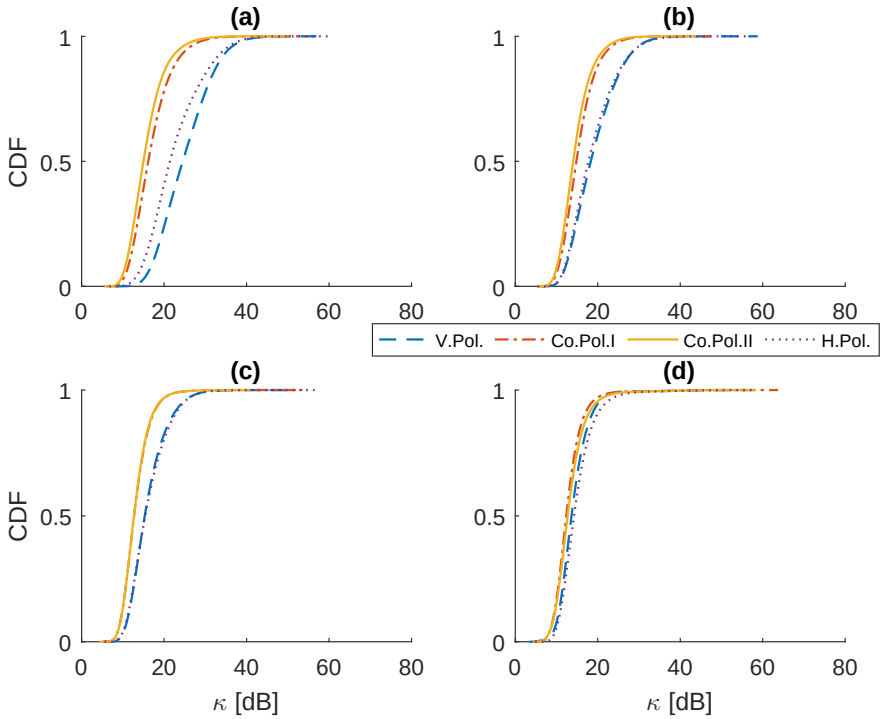

Figure 5.4: Condition number for different BS antenna array aperture: a) 0.17 m, b) 0.34 m, c) 1.5 m and d) 12 m

This behavior can be validated by studying the Cumulative Distribution Function (CDF) of the condition number of the channel κ, for the different BS antenna array aperture values, see Figure 5.4, where we observe that:

- For BS antenna array aperture of 0.17 m, Figure 5.4.a, κ has significantly different values for different antenna configurations.

- For BS antenna array aperture of 1.5 m, Figure 5.4.c, κ of the Co.Pol.I and Co.Pol.II configurations are similar but has a significant difference from the single-polarized configurations.
- For large BS antenna array aperture value (12 m), Figure 5.4.d, κ is almost similar for all antenna configurations.

Table 5.1: Summary of antenna element polarization and array aperture effect on sum-rate capacity

Analysis	Array Aperture(m)	V. Pol. Capacity (bits/s/Hz)	Co.Pol.II Capacity (bits/s/Hz)	% Capacity change (V. & Co. Pol.II)
MU-MISO	0.17	4.7	6.3	34
	0.34	5.67	6.55	15
	0.75	5.98	6.64	11
	1.5	6.27	6.8	8
	3	6.47	6.86	6
	6	6.66	6.95	4
	12	6.83	6.79	1
	24	6.67	6.62	1
MU-MIMO	0.17	6.12	8.83	44
	0.34	7.78	9.24	19
	0.75	8.30	9.45	14
	1.5	8.78	9.76	11
	3	9.14	9.9	8
	6	9.4	9.97	6
	12	9.81	9.76	1
	24	9.52	9.49	0

The sum-rate capacity improvement results for V.Pol. and Co.Pol.II configurations of setup-I is summarized in table 5.1.

5.2 Setup-IIA: Two BSs with fixed aperture

As described in section 3.3 the BS array size was fixed, so impact on total array size was not evaluated from this measurement data. Since the two BSs are located on two different buildings, this arrangement can be considered as coordinated multipoint MIMO, where JT/JP technique is assumed in this work.

5.2.1 Normalization

To study the effect of two BS antennas, a different normalization strategy was taken. One key assumption was that each BS has individual power control mech-

anism to compensate for the power differences beyond 1 m distance. Keeping this assumption in mind, the channel matrix was divided according to the BSs. Each part of the channel matrix was normalized by using Equation (5.1) by adjusting respective parameters. After normalization, both part of the channel matrix was placed together for analysis.

5.2.2 Results and analysis

MU-MISO

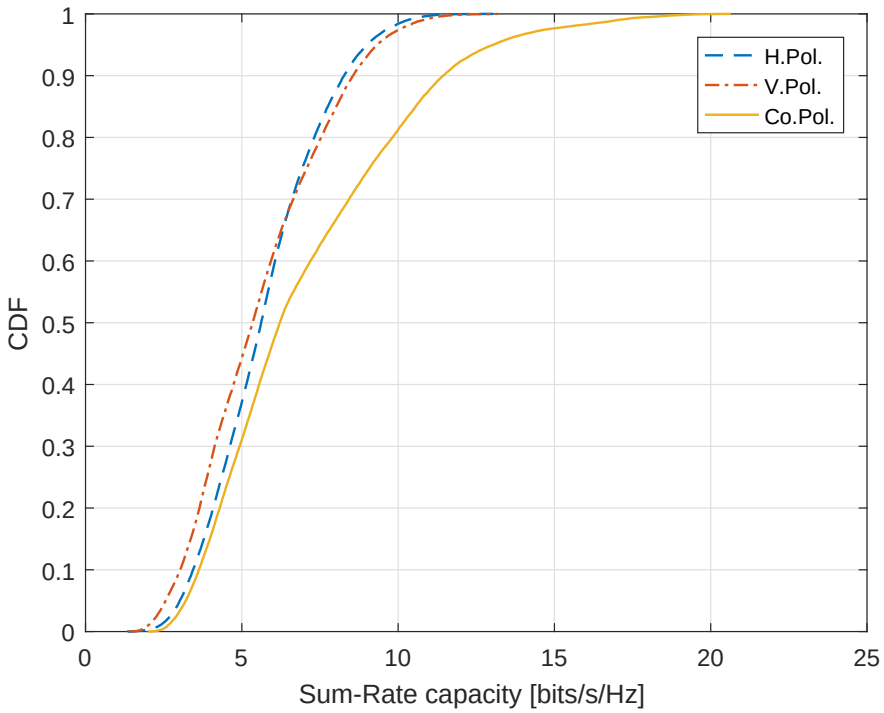

Figure 5.5: CDFs of sum-rate Capacity (MU-MISO)

The impact of antenna polarization on sum-rate capacity was investigated and presented in Figure 5.5. Here, it was found that, the cross-polarized configurations give an average sum-rate capacity increase of 27% compared to the single polarized antenna configurations.

MU-MIMO

Figure 5.6 depicts the impact of antenna polarization on sum-rate capacity. Here, it can be found that, the cross-polarized configurations give an average sum-rate

capacity increase of 39% compared to the single polarized antenna configurations.

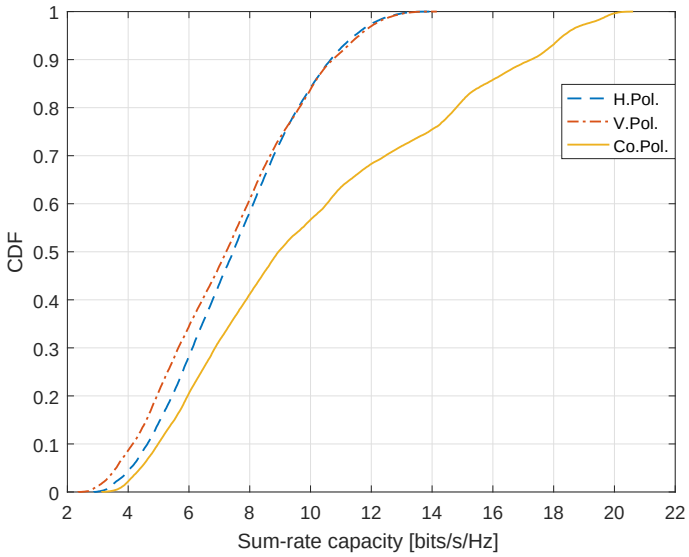

Figure 5.6: CDF of sum-rate capacity (MU-MIMO)

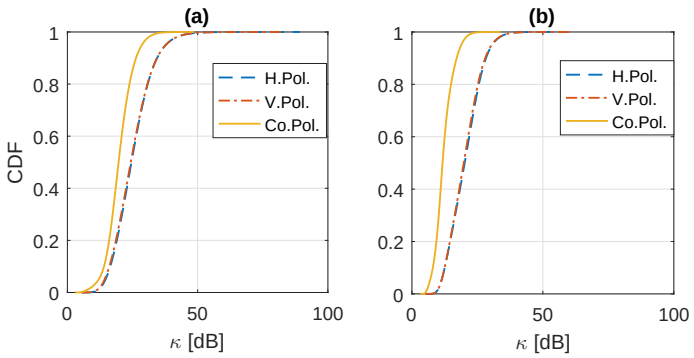

Figure 5.7: Condition number (singular value spread) of the channels, (a) MU-MISO, (b) MU-MIMO

The sum-rate capacity improvement for MU-MISO and MU-MIMO can be motivated by observing the channel condition number as shown in Figure 5.7. The CDF of the channel condition number for the cross-polarized antennas is 5 dB (Figure 5.7 (a)) and 8 dB (Figure 5.7 (b)) better for MU-MISO and MU-MIMO, respectively, compared to that of the single-polarized antennas. A similarity in channel condition number for single polarized antennas (H.Pol. and V.Pol. plots in Figure 5.7) can be observed which justifies the corresponding similarity of sum-rate capacity for these configurations (H.Pol. and V.Pol. plots in Figure 5.6).
Comparing Figure 5.5 and Figure 5.6, it can be observed that the ergodic sum-rate capacity for the cross-polarized antenna increases by 43% when the number of user antenna is increased from 1 to 2.
The sum-rate capacity improvement results of setup-IIA is summarized in table 5.2.

Table 5.2: Summary of antenna element polarization effect on sum-rate capacity for Setup-IIA

Analysis	H.Pol. Capacity (b/s/Hz)	V.Pol. Capacity (b/s/Hz)	Co.Pol. Capacity (b/s/Hz)	% Capacity change (single pol. & Co. Pol.)
MU-MISO	5.74	5.58	7.06	27
MU-MIMO	7.55	7.31	10.12	39

5.3 Setup-IIB: Two BSs with fixed aperture & user antenna pattern

As mentioned previously, the difference between setup-IIA and setup-IIB is in the user side, thus normalization description and assumptions made regarding the BSs of Setup-IIA is valid for Setup-IIB as well. Furthermore, MU-MISO configurations are not considered for the latter setup. The MIMO channel is constructed using the parameters of the MPCs and measured antenna patterns at different user positions where the effect of the user hand is included.

5.3.1 Results and analysis

Talk mode

In order to gain insight regarding the spatial structure of the channel, a few similarity metrics were analyzed. Figure 5.8 depicts the collinearity parameter of the channel for Talk mode position. As described earlier in Chapter 2, a collinearity value close to zero represents an orthogonal channel. As can be seen from Figure 5.8, the CDF for cross-polarized antenna configuration is closest to zero followed by CDFs of V.Pol. and H.Pol. configurations. This implies that the channels

between two users are more orthogonal and therefore have better separability of users and higher sum-rate capacity for the cross-polarized configuration.

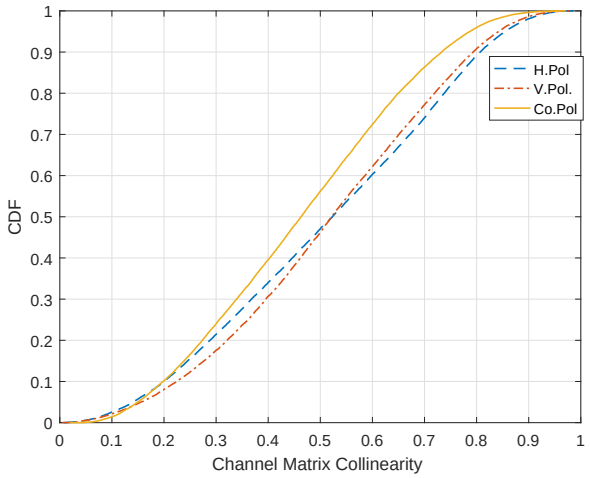

Figure 5.8: CDF of Channel Matrix Collinearity (Talk Mode)

For further analysis of the similarity of the channels, the condition number ratio metric was analyzed.

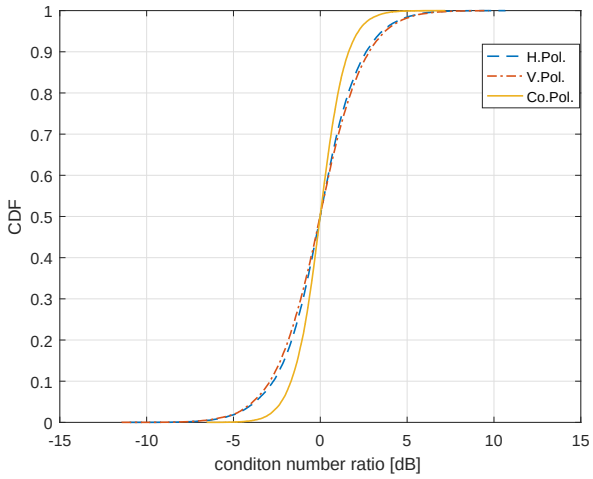

Figure 5.9: CDF of Condition Number Ratio (Talk Mode)

The ratio of the condition number for talk mode is presented in Figure 5.9. It was found that the standard deviations of the curves plotted in Figure 5.9 are 2.1918, 2.3062, 1.3497 for H.Pol., V.Pol. and Co. Pol. configurations, respectively. It is

evident that CDF of the Co.Pol. configuration has the smallest standard deviation, indicating a more stable channel similarity (mean of the CDFs) under this configuration.

Enriching the knowledge about the spatial structure of the channel, the sum-rate capacities were calculated as plotted in Figure 5.10.

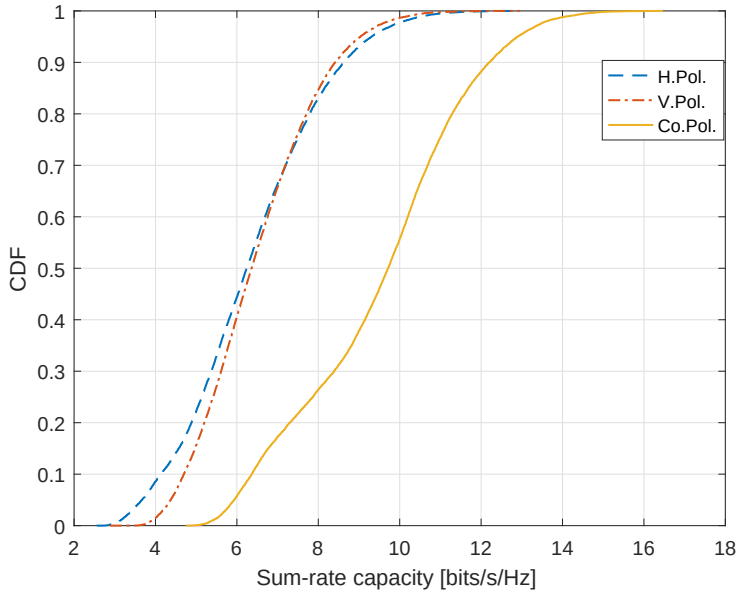

Figure 5.10: CDF of sum-rate capacity (Talk Mode)

From Figure 5.10 it can be found that the ergodic sum-rate capacity for the Co.Pol. configuration is around 50% and 46% higher than that of the H.Pol. and V.Pol. configurations, respectively. This is commensurate with the findings about the spatial structure of the channels. However, since sum-rate capacity is calculated from the equivalent channel as described in the table 4.1, the properties of these equivalent channels were studied also.

In Figure 5.11 the channel condition number (singular value spread) has been plotted. It can be seen that the condition number for the Co.Pol. configuration is closer to zero, representing a well-balanced channel. For further illustration, the singular value ratios of the channels for different configurations are observed and plotted in Figure 5.12.

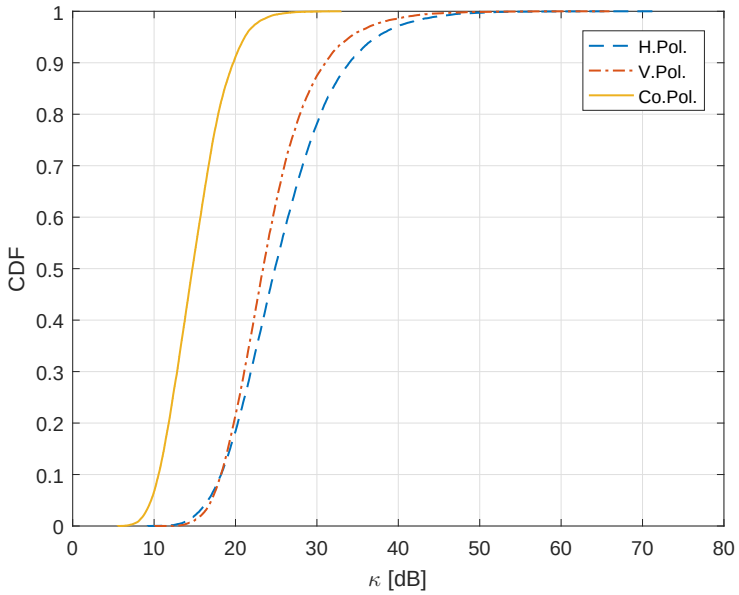

Figure 5.11: CDF of the condition numbers of the equivalent channels

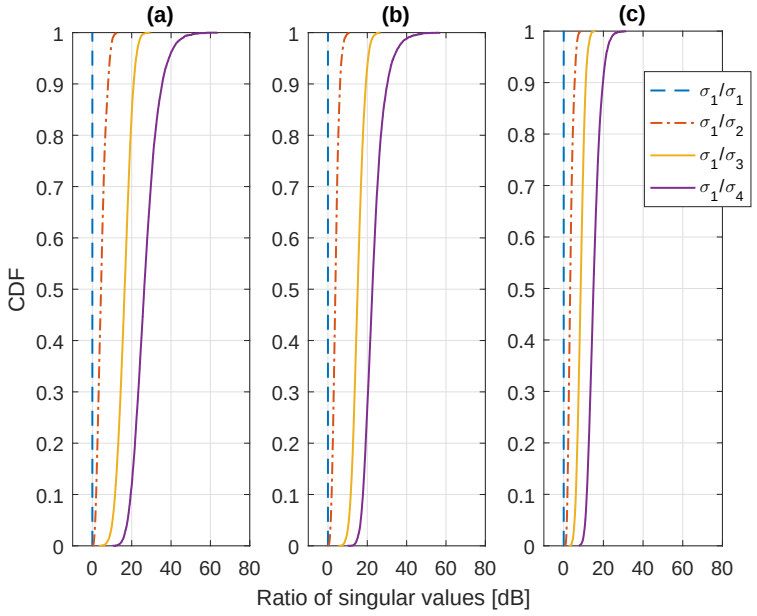

Figure 5.12: CDF of Ratio of the Singular values (Talk Mode), (a) H.Pol. (b) V.Pol. (c) Co.Pol. configurations

As can be seen from Figure 5.12 the difference between the ratio of singular values for the Co.Pol configuration is the least, which represents a higher rank channel providing better sum-rate capacity.

Browse mode

Same analysis as in talk mode were performed for the browse mode as well. The channel matrix collinearity for the browse mode is presented in Figure 5.13.

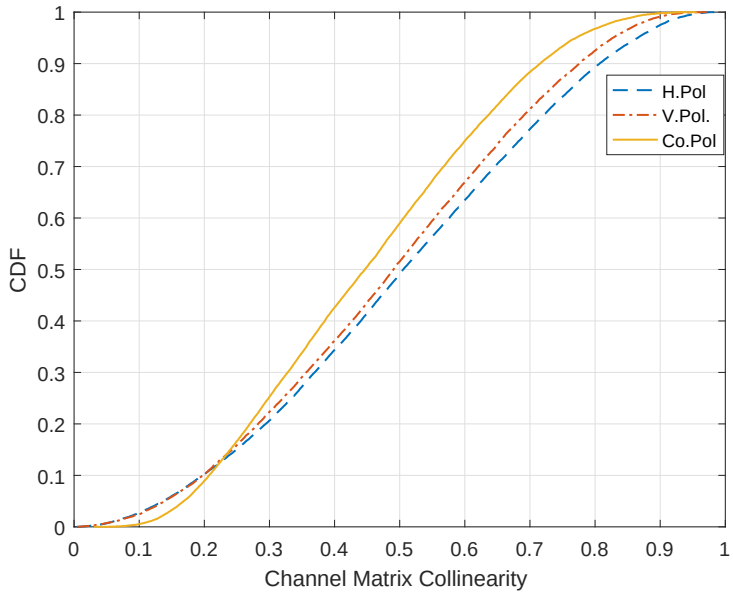

Figure 5.13: CDF of Channel Matrix Collinearity (Browse mode)

Similar to Figure 5.8, in Figure 5.13 it is evident that the channels between two users for Co.Pol. configuration are more orthogonal compared to that of the H.Pol. and V.Pol. configurations.

The channel condition number ratio for the browse mode was also calculated as shown in Figure 5.14. The standard deviation of the curves of Figure 5.14 are 2.3006, 2.2565, 1.4146 for V.Pol. H.Pol. and Co.Pol configurations, respectively. Hence, similar conclusions for browse mode regarding the channel structure can be made as was done previously for talk mode position. However, no attempts were made to quantify the relation between the spatial structures of the channels for talk mode and browse mode.

The sum-rate capacity of the browse mode was found and the CDF is plotted in Figure 5.15.The mean value of the Co.Pol. configuration was found to be 51% and 24% better than the H.Pol. and V.Pol. configuration, respectively.

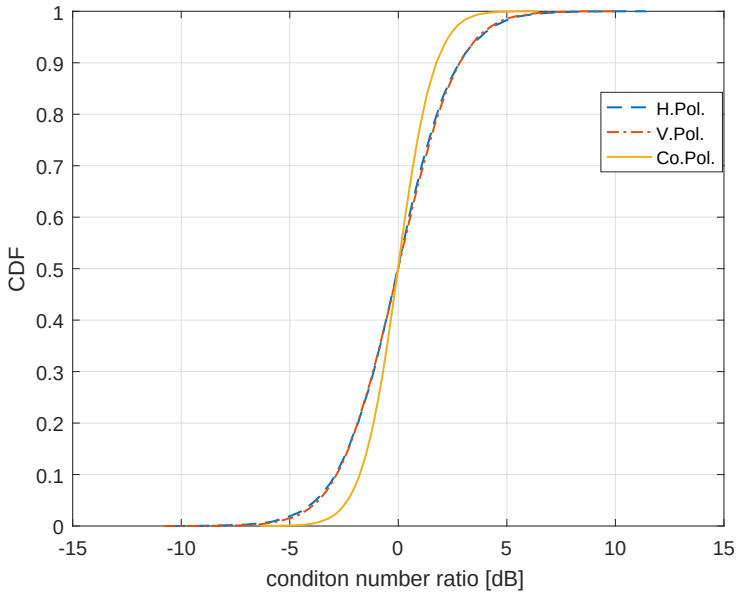

Figure 5.14: CDF of Condition Number Ratio (Browse mode)

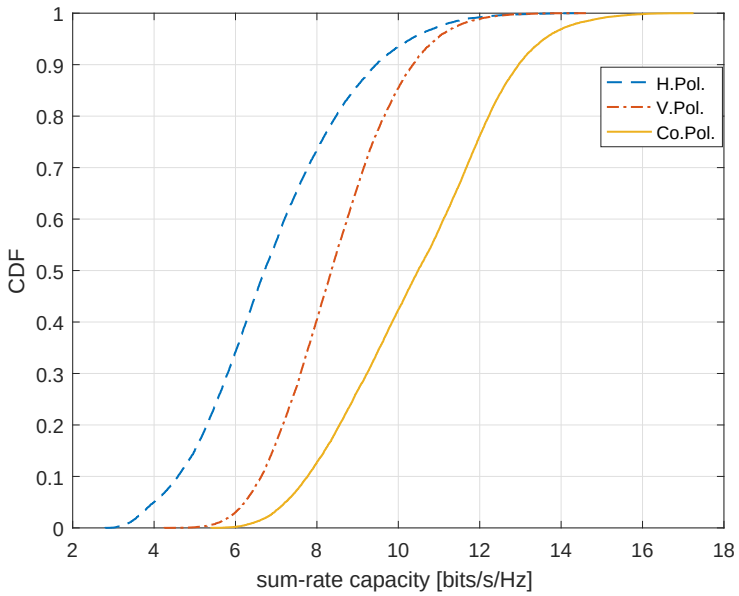

Figure 5.15: CDF of sum-rate capacity (Browse mode)

To support the sum-rate capacity improvements, analysis such as; condition num-

ber analysis and ratio of the singular values, were performed on the equivalent channels for the browse mode. Figures 5.16 and 5.17 show the plots for condition number analysis and ratio of the singular values, respectively.

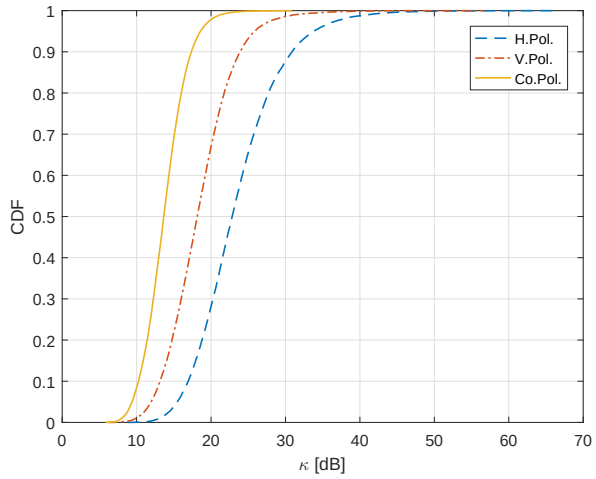

Figure 5.16: CDF of the condition numbers of the equivalent channels

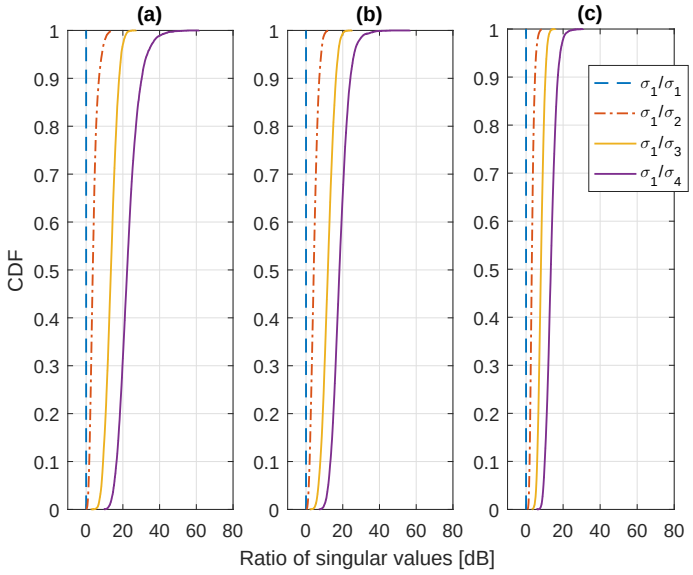

Figure 5.17: CDF of Ratio of the Singular values(Browse Mode), (a) H.Pol. (b) V.Pol. (c) Co.Pol. configurations

The sum-rate capacity improvement between V.Pol. and Co.Pol. configurations for talk mode was 46% while for browse mode the improvement was only 24%. Dissimilarity between the CDFs for V.Pol. in Figure 5.11, and Figure 5.16 confirms this difference in sum-rate capacity improvements. The sum-rate capacities for setup-IIB are summarized in table 5.3.

Table 5.3: Summary of antenna element polarization effect on sum-rate capacity for Setup-IIB

Mode	H.Pol. Capacity (b/s/Hz)	V.Pol. Capacity (b/s/Hz)	Co.Pol. Capacity (b/s/Hz)	% Capacity change (H. pol. & Co. Pol.)	% Capacity change (V.Pol & Co.Pol.
Talk	6.35	6.49	9.49	50	46
Browse	6.9	8.44	10.45	51	24
% change between Talk and Browse mode	9	30	10		

It can be observed from table 5.3 that the sum-rate capacities for browse mode is better than that of the talk mode for the same propagation channel [1]. This difference in sum-rate capacity can be attributed to the different radiation patterns plotted in Figures 3.13 and 3.15 which changes the effective radio channel between the BS and the user.

[1] Although the radio channel is different. Difference between propagation channel and radio channel can be found in [17]

Chapter 6

Conclusion

This work has investigated the effect of antenna polarization and antenna array size on the sum-rate capacity of a CoMP system, using measured channels and including the effect of the body of the user on the MS antenna pattern.

Case 1:

Having only one BS with limited number of antennas and variable aperture size, the following sum-rate capacity analysis for single and cross-polarized antennas were evaluated.

MU-MISO

Varying BS antenna array size from 0.17 m to 12 m improves sum-rate capacity of the MIMO channel by 48% and 14% for vertical and cross-polarized antennas, respectively. Furthermore, the difference in sum- rate capacity performance between various polarizations is apparent while the antenna array size is small. This behavior was motivated by studying the condition number of the channel where it was shown that the condition number was significantly different for different antenna polarization at small antenna array size while this distinction diminished with increasing the array size.

MU-MIMO

A sum-rate capacity increase of 60% and 19% was observed for vertical and cross-polarized antennas, respectively, while the array size was varied from 0.17 m to 12 m. Changing the array size has distinct effect on the sum-rate capacity for different antenna polarizations as was explained for MU-MISO above.
Additionally, 44% and 34% increase in the sum-rate capacity for MU-MIMO and MU-MISO, respectively was observed by using cross-polarized antennas at the BS when the total antenna array aperture was limited to 0.17 m.

Case 2:

Having two BSs with limited number of antennas and inter-BS distance (i.e. fixed array size) of 60 m, the following sum-rate capacity analysis for single- and cross-polarized antennas were performed. This analysis does not include the user hand effect on the performance of MIMO channel.

MU-MISO & MU-MIMO

Cross-polarized patch antennas enhanced the sum-rate capacity by 27% and 39% compared to single polarized antennas, for MU-MISO and MU-MIMO, respectively. The distribution of the channel condition numbers showed noticeable difference amongst different antenna polarizations. The CDF of the channel condition number for the cross-polarized antennas is 5 dB and 8 dB better for MU-MISO and MU-MIMO, respectively, compared to that of the single polarized antennas. Increasing number of user antenna elements from one to two increased the sum-rate capacity by 43%.

Case 3:

Having two BSs with limited number of antennas and inter-BS distance (i.e. fixed array size) of 60 m, the following sum-rate capacity conclusion for talk and browse mode, i.e. including user hand effect, were reached.

Talk Mode

Cross-polarized antennas yield higher sum-rate capacity by 50% and 46% compared to that of horizontal and vertical polarized antennas, respectively. Evaluation of few channel metrics, such as collinearity, singular value spread and ratio of condition numbers, supported the sum-rate capacity gain results.

Browse Mode

Similar analysis as in talk mode were performed for the browse mode as well. Sum-rate capacity improvement of about 51% and 24% was observed for cross-polarized antennas compared to horizontal and vertical polarized antennas, respectively. Same analysis on the channel, as in the talk mode, justified the results.

Chapter 7

Future works

Although this thesis work shows the effect of antenna polarization on the ergodic sum-rate capacity of CoMP systems quantitatively in the measurement environment for densly spaced users, a few extensions of the work can be performed to further analyze the results.

Use of power optimization algorithms

One of the key assumptions of this work while evaluating the sum-rate capacity, is equal power allocation. Optimized algorithms such as water-filling [1] can be used to maximize the capacity.

Use of optimal precoding algorithms

Only linear precoding schemes such as MMSE, ZF precoding were used in this work. However, alternative linear techniques such as optimal linear precoders [28] and nonlinear precoding such as Tomlinson-Harashima precoding can be implemented.

Use of different coordination techniques

Instead of using JT/JP CoMP techniques at the BSs, CS/CB coordination can be studied as this reduces the amount of load on the backbone.

Bibliography

[1] A. Paulraj, R. Nabar, and D. Gore, *Introduction to Space-Time Wireless Communications*. New York: Cambridge University Press, 2008.

[2] A. F. Molisch, *Wireless Communications*. West Sussex: John Wiley & Sons, 2011.

[3] B. Z. Maha and R. Kosai, *Multi User MIMO Communication: Basic Aspects, Benefits and Challenges, Recent Trends in Multi-user MIMO Communications*. Intech, 2013.

[4] G. Bauch and A. Alexiou, "MIMO technologies for the wireless future," in *Personal, Indoor and Mobile Radio Communications, 2008. PIMRC 2008. IEEE 19th International Symposium on*, pp. 1–6, Sept 2008.

[5] D. Gesbert, M. Kountouris, R. W. H. Jr., C. b. Chae, and T. Salzer, "Shifting the MIMO paradigm," *IEEE Signal Processing Magazine*, vol. 24, pp. 36–46, Sept 2007.

[6] C. Yang, S. Han, X. Hou, and A. F. Molisch, "How do we design CoMP to achieve its promised potential?," *IEEE Wireless Communications*, vol. 20, pp. 67–74, February 2013.

[7] Z. Chen, M. Peng, W. Wang, and H. Chen, "Cooperative base station beamforming in WiMAX systems," *IET Communications*, vol. 4, pp. 1049–1058, June 2010.

[8] M. K. Karakayali, G. J. Foschini, and R. A. Valenzuela, "Network coordination for spectrally efficient communications in cellular systems," *IEEE Wireless Communications*, vol. 13, pp. 56–61, Aug 2006.

[9] R. Irmer, H. Droste, P. Marsch, M. Grieger, G. Fettweis, S. Brueck, H. P. Mayer, L. Thiele, and V. Jungnickel, "Coordinated multipoint: Concepts, performance, and field trial results," *IEEE Communications Magazine*, vol. 49, pp. 102–111, February 2011.

[10] J. Lee, Y. Kim, H. Lee, B. L. Ng, D. Mazzarese, J. Liu, W. Xiao, and Y. Zhou, "Coordinated multipoint transmission and reception in LTE-advanced systems," *IEEE Communications Magazine*, vol. 50, pp. 44–50, November 2012.

[11] M. S. Ali, "On the Evolution of Coordinated Multi-Point (CoMP) Transmission in LTE-Advanced," *International Journal of Future Generation Communication and Networking*, vol. 7, no. 4, pp. 91–102, 2014.

[12] D. Lee, H. Seo, B. Clerckx, E. Hardouin, D. Mazzarese, S. Nagata, and K. Sayana, "Coordinated multipoint transmission and reception in LTE-advanced: deployment scenarios and operational challenges," *IEEE Communications Magazine*, vol. 50, pp. 148–155, February 2012.

[13] B. K. Lau, M. A. Jensen, J. Medbo, and J. Furuskog, "Single and Multi-User Cooperative MIMO in a Measured Urban Macrocellular Environment," *IEEE Transactions on Antennas and Propagation*, vol. 60, pp. 624–632, Feb 2012.

[14] V. Jungnickel, S. Jaeckel, L. Thiele, L. Jiang, U. Kruger, A. Brylka, and C. von Helmolt, "Capacity Measurements in a Cooperative MIMO Network," *IEEE Transactions on Vehicular Technology*, vol. 58, pp. 2392–2405, Jun 2009.

[15] G. Dahman, J. Flordelis, and F. Tufvesson, "Experimental evaluation of the effect of BS antenna inter-element spacing on MU-MIMO separation," in *Communications (ICC), 2015 IEEE International Conference on*, pp. 1685–1690, June 2015.

[16] F. Harrysson, J. Medbo, A. F. Molisch, A. J. Johansson, and F. Tufvesson, "Efficient experimental evaluation of a MIMO handset with user influence," *IEEE Transactions on Wireless Communications*, vol. 9, pp. 853–863, February 2010.

[17] B.Clerckx and C. Oestges, *MIMO Wireless Networks Channels, Techniques and Standards for Multi-Antenna, Multi-User and Multi-Cell Systems*. Oxford: Academic Press, 2013.

[18] B. H. Fleury, X. Yin, K. G. Rohbrandt, P. Jourdan, and A. Stucki, "Performance of a high-resolution scheme for joint estimation of delay and bidirection dispersion in the radio channel," in *Vehicular Technology Conference, 2002. VTC Spring 2002. IEEE 55th*, vol. 1, pp. 522–526 vol.1, 2002.

[19] N. Czink, B. Bandemer, G. Vazquez-Vilar, L. Jalloul, C. Oestges, and A. Paulraj, "Spatial separation of multi-user MIMO channels," in *2009 IEEE 20th International Symposium on Personal, Indoor and Mobile Radio Communications*, pp. 1059–1063, Sept 2009.

[20] J. Flordelis, X. Gao, G. Dahman, F. Rusek, O. Edfors, and F. Tufvesson, "Spatial separation of closely-spaced users in measured massive multi-user MIMO channels," in *2015 IEEE International Conference on Communications (ICC)*, pp. 1441–1446, June 2015.

[21] R. S. Thoma, D. Hampicke, A. Richter, G. Sommerkorn, A. Schneider, and U. Trautwein, "Identification of time-variant directional mobile radio channels," in *Instrumentation and Measurement Technology Conference, 1999. IMTC/99. Proceedings of the 16th IEEE*, vol. 1, pp. 176–181 vol.1, 1999.

[22] J. Flordelis, G. Dahman, and F. Tufvesson, "Measurements of large-scale parameters of a distributed MIMO antenna system in a microcell environment at 2.6 Ghz," in *Antennas and Propagation (EuCAP), 2013 7th European Conference on*, pp. 3026–3030, April 2013.

[23] G. Caire and S. S. Shamai, "On achievable rates in a multi-antenna broadcast downlink," in *ALLERTON 2000, 38th Annual Allerton Conference on Communications, Control and Computing, Monticello, October 4-6, 2000, Monticello, USA*, (Monticello, UNITED STATES), 10 2000.

[24] M. Costa, "Writing on dirty paper (Corresp.)," *IEEE Transactions on Information Theory*, vol. 29, pp. 439–441, May 1983.

[25] S. Vishwanath, N. Jindal, and A. Goldsmith, "Duality, achievable rates, and sum-rate capacity of Gaussian MIMO broadcast channels," *IEEE Transactions on Information Theory*, vol. 49, pp. 2658–2668, Oct 2003.

[26] W. Yu and J. M. Cioffi, "Sum capacity of Gaussian vector broadcast channels," *IEEE Transactions on Information Theory*, vol. 50, pp. 1875–1892, Sept 2004.

[27] Q. H. Spencer, A. L. Swindlehurst, and M. Haardt, "Zero-forcing methods for downlink spatial multiplexing in multiuser MIMO channels," *IEEE Transactions on Signal Processing*, vol. 52, pp. 461–471, Feb 2004.

[28] Q. H. Spencer, J. Wallace, C. Peel, T.Svantesson, A. L. Swindlehurst, and A. Gummala, "Performance of multi-user spatial multiplexing with measured channel data," in *MIMO System Technology and Wireless communications* (G. Tsoulos, ed.), ch. 7, pp. 175–206, Boca Raton: CRC Press, 2006.

[29] F. Kaltenberger, M. Kountouris, D. Gesbert, and R. Knopp, "On the trade-off between feedback and capacity in measured MU-MIMO channels," *IEEE Transactions on Wireless Communications*, vol. 8, pp. 4866–4875, September 2009.

LUND
UNIVERSITY

Series of Master's theses
Department of Electrical and Information Technology
LU/LTH-EIT 2016-500

http://www.eit.lth.se